JOURNAL OF GEOPHYSICAL RESEARCH, VOL. 113, A04204, doi:10.1029/2007JA012604, 2008

Solar wind plasma entry into the magnetosphere under northward IMF conditions

Wenhui Li,[1] Joachim Raeder,[1] Michelle F. Thomsen,[2] and Benoit Lavraud[2]

Received 21 June 2007; revised 18 October 2007; accepted 18 December 2007; published 3 April 2008.

[1] This study examines how solar wind plasma enters the magnetosphere under northward interplanetary magnetic field (IMF) conditions, using the Open Geospace General Circulation Model (OpenGGCM) for various solar wind, IMF, and geomagnetic dipole conditions. We trace flow paths of individual fluid elements from the solar wind and study the variation of the topology of the magnetic field line along those flow paths. We find that there is an entry window through which the solar wind plasma can enter the magnetosphere as a result of double high-latitude reconnection under northward IMF conditions. We investigate how the entry window depends on solar wind, IMF, and geomagnetic dipole parameters, and we estimate the solar wind plasma entry rate for various conditions. We find that the effective entry rate under northward IMF conditions is of the order of 10^{26} to 10^{27} particles per second. We also estimate the conditions for which solar wind plasma entry is most efficient. The newly created flux tubes with closed-field topology are subsequently convected to the nightside and consequently cause magnetosheath plasma to be captured and enter the magnetosphere. Some captured dayside plasma takes about 90 min to convect along the magnetopause to a near tail flank region of the central plasma sheet, thus forming a cold dense plasma sheet. Double high-latitude reconnection can also release the captured plasma. Thus a balance of inflow and outflow of the captured plasma is eventually established under prolonged northward IMF conditions. We find that high-latitude reconnection is common under northward IMF conditions in our simulations. It occurs for IMF with any clock angle within $[-90°, 90°]$, measured in front of the bow shock, and for any geomagnetic dipole tilt angle within $[-30°, 30°]$. An IMF field line with a zero x component usually first reconnects with a geomagnetic field line at the northern high-latitude boundary when the geomagnetic dipole tilts positive toward the Sun, and vice versa for negative dipole tilt. Our simulations also show that ionosphere conductance affects the convection of the newly closed field lines. Consequently, ionosphere conductance can change the solar wind plasma effective entry rate and can cause asymmetric effective entry rate with respect to positive and negative IMF clock angles.

Citation: Li, W., J. Raeder, M. F. Thomsen, and B. Lavraud (2008), Solar wind plasma entry into the magnetosphere under northward IMF conditions, *J. Geophys. Res.*, *113*, A04204, doi:10.1029/2007JA012604.

1. Introduction

[2] Magnetic reconnection plays a dominant role in bringing solar wind mass and energy into the Earth's magnetosphere and down to the ionosphere. When the interplanetary magnetic field (IMF) is southward, solar wind plasma can enter into the plasma sheet through reconnection processes first at the dayside subsolar merging site and then in the distant magnetotail [*Dungey*, 1961; *Cowley*, 1980; *Rosenbauer et al.*, 1975; *Sckopke et al.*, 1981]. Under northward IMF conditions, magnetic reconnection occurring tailward of the cusp has been found to be a critical process that leads to the formation of the low-latitude boundary layer (LLBL) [*Cowley*, 1981; *Song and Russell*, 1992; *Le et al.*, 1996] and the formation of the cold dense plasma sheet (CDPS) [*Raeder et al.*, 1997; *Øieroset et al.*, 2005; *Li et al.*, 2005].

[3] *Dungey* [1963] first proposed that a northward IMF would be antiparallel to the Earth's field at points poleward of the cusps and make reconnection possible there. Such reconnection is usually called high-latitude reconnection. *Russell* [1972] proposed that the IMF field lines interconnect with open tail lobe field lines rather than with closed field lines in either one hemisphere or the other. For a tilted geomagnetic field, *Cowley* [1981, 1983] suggested that a northward IMF field line may merge with a closed geomagnetic field line in the northern hemisphere of a closed

[1]Space Science Center, University of New Hampshire, Durham, New Hampshire, USA.
[2]Space Science and Applications, Los Alamos National Laboratory, Los Alamos, New Mexico, USA.

0148-0227/08/2007JA012604$09.00

magnetosphere, forming an open field line that drapes over the dayside magnetopause and another open field line that connects to the southern hemisphere. After some time, the ''overdraped'' open field line merges with one of the previously opened field lines in the southern hemisphere, creating a new closed dayside field line and a completely detached field line.

[4] Global magnetosphere MHD models have reproduced high-latitude reconnection under northward IMF conditions [*Ogino et al.*, 1994; *Fedder and Lyon*, 1995; *Raeder et al.*, 1997; *Gombosi et al.*, 1998; *Song et al.*, 1999; *Guzdar et al.*, 2001]. Observational evidence in support of this process has also been presented [*Omelchenko et al.*, 1983; *Gosling et al.*, 1991; *Kessel et al.*, 1996; *Matsuoka et al.*, 1996; *Fuselier et al.*, 2000; *Le et al.*, 2001; *Onsager et al.*, 2001; *Phan et al.*, 2003; *Lavraud et al.*, 2002, 2004, 2005a]. From the three-dimensional electron and ion distribution measured by the Polar Hydra instrument, *Onsager et al.* [2001] identified several distinct boundary layer regions associated with the high-latitude reconnection processes under northward IMF conditions: (1) the cusp; (2) the magnetopause current layer; (3) magnetosheath field lines that have interconnected only in the Northern Hemisphere; (4) magnetosheath field lines that have interconnected only in the Southern Hemisphere; (5) magnetosheath field lines that have interconnected in both the Northern and Southern Hemispheres; (6) magnetosheath that is disconnected from the terrestrial magnetic field; and (7) high-latitude plasma sheet field lines that are participating in magnetosheath reconnection. *Onsager et al.* [2001] suggested that the high-latitude plasma sheet field lines present at the high-latitude magnetopause could possibly be a result of the erosion of the flank lobes by high-latitude reconnection. They also found that reconnection during a northward IMF time period occurred at high latitudes over a broad local time extent, interconnecting magnetosheath and lobe and/or plasma sheet field lines in both the Northern and Southern Hemispheres. Newly closed boundary layer field lines were observed as reconnection occurred first at high latitudes in one hemisphere and then later in the other. This scenario was further confirmed statistically by *Lavraud et al.* [2005a, 2005b].

[5] High-latitude reconnection has been proposed as a mechanism for the formation of the low-latitude boundary layer under northward IMF conditions [e.g., *Cowley*, 1981; *Song and Russell*, 1992]. From ISEE observations, *Le et al.* [1996] showed that there are two types of low-latitude boundary layer plasma for a northward interplanetary magnetic field: (1) an outer boundary layer, where both heated magnetosheath plasma is the dominant particle population and the hot magnetospheric component is strongly depleted or missing; and (2) an inner boundary layer where the two components are more nearly equal. The two types of plasma characteristics can be explained by the process of magnetic reconnection poleward of the cusp. *Le et al.* [1996] interpreted the outer boundary layer as a layer composed of open field lines that are formed by magnetic reconnection above one cusp. The inner boundary layer is composed of newly closed field lines that are formed from magnetosheath field lines by double magnetic reconnection, first poleward of one cusp and later poleward of the other cusp. In a 3-D hybrid simulation, *Lin and Wang* [2006] showed that as a result of the double high-latitude reconnection process, a thick magnetopause boundary layer is formed by the magnetosheath ions captured on the newly closed field lines and the transmitted magnetosheath ions near the high-latitude X lines.

[6] The high-latitude reconnection process is also an important mechanism that causes the solar wind plasma and energy to penetrate the magnetosphere. It has been observed that the plasma sheet becomes colder and denser when the IMF is northward for at least several hours [e.g., *Fairfield et al.*, 1981; *Baumjohann et al.*, 1989; *Lennartsson*, 1992; *Fujimoto et al.*, 1996, 1998; *Terasawa et al.*, 1997]. The source of the cold dense plasma sheet (CDPS) is believed to be the solar wind. A number of processes have been proposed to account for the transfer of solar wind plasma into the magnetosphere [e.g., *Sibeck et al.*, 1999; *Hultqvist et al.*, 1999; *Walker et al.*, 1999], including direct cusp entry, finite gyroradii effect, wave-particle interaction, turbulence, and impulsive penetration [*Axford and Hines*, 1961; *LeMaire*, 1977; *Treumann*, 1997; *Thorne and Tsurutani*, 1991; *Tsurutani et al.*, 2003]. Using global MHD simulations together with single particle trajectory calculations, *Walker et al.* [2003] showed that solar wind ions enter the magnetosphere as a result of high-latitude reconnection in both cusps when the IMF is purely northward. The following two mechanisms are considered to be the main processes that can transport the magnetosheath plasma into the magnetosphere under northward IMF conditions:

[7] 1. The first mechanism is high-latitude reconnection in both hemispheres that captures magnetosheath flux tubes at the dayside magnetopause [*Onsager et al.*, 2001; *Lavraud et al.*, 2006]. The captured flux tubes then are convected into the tail [*Song and Russell*, 1992; *Raeder et al.*, 1995, 1997; *Li et al.*, 2005].

[8] 2. The second is diffusion processes facilitated by the Kelvin-Helmholtz instability that allows magnetosheath plasma to diffuse across the boundary [*Terasawa et al.*, 1997; *Fairfield et al.*, 2000; *Fujimoto and Terasawa*, 1994; *Nykyri and Otto*, 2001; *Nykyri et al.*, 2006; *Hasegawa et al.*, 2004].

[9] In studying the cold dense plasma sheet event on 23 October 2003 through the analysis of a global MHD simulation, *Li et al.* [2005] showed that flow paths exist that allow solar wind plasma fluid elements to enter the magnetosphere. The solar wind fluid element is slightly heated and accelerated near the high-latitude reconnection location and flows to the location where Cluster observed the cold dense plasma sheet in the near tail. This study also revealed that double high-latitude reconnection creates new closed flux tubes, which are composed of a section of the magnetosheath flux tube at the dayside magnetopause and two sections of geomagnetic flux tubes from both hemispheres. After their creation, the two kinked sections of the newly closed flux tube are first driven sunward along the dayside magnetopause by the $\mathbf{J} \times \mathbf{B}$ force. Subsequently, the whole new flux tube is contracted into the magnetosphere and is convected to the magnetotail. The simulation indicates that such a capturing mechanism is sufficient to form the observed cold dense plasma sheet.

[10] *Pilipp and Morfill* [1978] estimated a solar wind entry rate of about 10^{26} to 10^{27} particles per second through the plasma mantle when the IMF is southward. *Cowley*

[1980] also gave an estimation of particle influx of about 10^{27} s^{-1} through the new open flux tubes created from dayside reconnection. For northward IMF conditions, *Eastman et al.* [1985] estimated that a few times 10^{26} particles per second enter the magnetosphere. *Richard et al.* [1994] calculated the total entry rate to be 1.7×10^{27} particles per second using test particle calculations for northward IMF conditions. These studies also estimated that a particle entry rate of 10^{27} s^{-1} is sufficient to fill and to maintain the plasma sheet. *Walker et al.* [2003], from their MHD simulation and single particle trajectory calculations, estimated the ion entry rate to be on the level of 10^{26}–10^{27} particles per second under northward IMF conditions.

[11] From a Cluster survey of high-latitude reconnection, *Twitty et al.* [2004] found a cusp reconnection occurrence rate of 90% when the IMF clock angle, measured by ACE, is between $-90°$ and $90°$. In another statistical study of the magnetosheath electron boundary layer using Cluster data, *Lavraud et al.* [2006] showed that double high-latitude reconnection occurs primarily when the magnetosheath magnetic field clock angle, measured by Cluster FGM, is in the interval of $[-60°, 60°]$. Cluster observations have also shown that the dipole tilt angle determines in which hemisphere high-latitude reconnection of a magnetosheath field line occurs first [*Lavraud et al.*, 2005b].

[12] Owing to the sparse spatial coverage of in situ observations, the behavior of the high-latitude reconnection and the solar wind plasma entry in relation to the solar wind and northward IMF conditions are still relatively poorly known. In the present study, motivated by the successful simulation presented by *Li et al.* [2005], we use the global magnetosphere MHD model Open Geospace General Circulation Model (OpenGGCM) [*Raeder et al.*, 1995; *Raeder*, 1999; *Raeder et al.*, 2001a; *Raeder*, 2003] to investigate the solar wind entry on a global scale and estimate the entry rate for various solar wind, geomagnetic dipole, and IMF conditions.

2. Simulation

[13] OpenGGCM solves the resistive MHD equations on a nonuniform rectilinear grid, with a minimum grid spacing at GSE $y = 0$ and $z = 0$ for the y direction and the z direction, respectively, and at a point near the dayside magnetopause for x direction. The outer boundary conditions on the dayside are the solar wind and IMF conditions, while those on the other five outer boundaries are free (i.e., normal derivatives vanish). The inner boundary conditions are derived from the coupling with an ionospheric model. Field-aligned currents (FAC) are computed just outside a spherical region of radius 3.5 R_E, centered around the Earth, and mapped to a spherical-polar ionosphere grid at 1 R_E using a dipole magnetic field model. The ionosphere potential is solved on the surface of a sphere with 1.02 R_E radius. The ionospheric electric field is mapped back to the surface of the sphere with 3.5 R_E radius. In a OpenGGCM simulation, the ionosphere can be either set simply to be a sphere with constant uniform conductance, modeled by empirical parameters [*Robinson et al.*, 1987], or modeled by the NOAA Coupled Thermosphere Ionosphere Model (CTIM) [*Fuller-Rowell et al.*, 1996]. A more detailed description of the OpenGGCM model and ionosphere coupling can be found in related articles [*Raeder et al.*, 1998, 2001a; *Raeder*, 2003].

[14] The OpenGGCM has been successfully used to simulate an event with extended period of northward IMF on 23 October 2003, during which a cold dense plasma sheet was observed by Cluster [*Li et al.*, 2005; *Øieroset et al.*, 2005]. Based on this simulation case study, we run a series of simulations using generic input parameters in which we vary the solar wind, IMF conditions, and the geomagnetic dipole tilt angle. In these simulations, the ionosphere model CTIM is coupled to provide inner boundary conditions [*Raeder et al.*, 2001b]. For the first 3 h of these simulations, the solar wind and IMF conditions are set to average values (velocity: 450 km/s, density: 6.6 cm^{-3}, pressure: 30 pPa, IMF: 7.0 nT) [*Kivelson and Russell*, 1995], and for the magnetosphere to form, the IMF direction is set to be pure southward. The IMF is then turned to northward at the magnetopause and other conditions are changed according to the parameter to be investigated, then kept constant until the end of a simulation. In our simulations, we only vary the geomagnetic dipole tilt angle in the GSE XZ plane, and set the angle constant during each simulation run. The x component of IMF, and y and z components of solar wind velocity are set to be zero for simplicity in all of these simulations.

3. Magnetic Field Line Topology and the Reconnection Process

[15] In our analysis, we trace fluid elements and the magnetic field flux tubes threading through them. We compute the path (not necessarily a streamline) of a fluid element starting from the solar wind in front of the bow shock at certain time, using the flow velocity field in the simulation domain at different output times, i.e.,

$$\frac{d\vec{X}(t)}{dt} = \vec{V}\left(\vec{X}(t), t\right). \tag{1}$$

[16] We use linear interpolation in both space and time to compute the velocity as well as other quantities in the simulation at a given location and a given time. We set the tracing time step, i.e., the iteration step, to be 2 s, corresponding to $\sim$0.14 R_E for a flow speed of 450 km/s or $\sim$0.03 R_E for a flow speed of 100 km/s. At each time step, we also calculate the magnetic field line threading through the fluid element and determine its topology (IMF, open or closed).

[17] Here we call the magnetic flux tube threading through a fluid element as its frozen-in magnetic field line (FIMFL), although such a flux tube may not be frozen in when the fluid element is in a region where the frozen-in condition is broken. Usually, a fluid element is considered to be a solar wind plasma element if its FIMFL's topology is IMF. It is identified as an element in the magnetosphere closed field region if its FIMFL's topology is closed. It is considered to be a lobe or mantle plasma element if its FIMFL's topology is open. Tracing a fluid element and identifying its FIMFL's topology at each iteration step, we are able to find out how a fluid element flows from one region to the other and how it crosses separatrices.

Table 1. Field Line Topology Classification

Name	Description
IMF1	Northward IMF field lines in the magnetosheath before any reconnection has occurred. They may drape over the magnetopause down to the near tail and be antiparallel to north and south lobe or mantle field lines at some point.
open1	Lobe or mantle field lines extending relatively straight tailward. They are the original lobe or mantle field lines, or new open field lines (see description of open2 and open3) that have been convected and stretched tailward. This open field line extends from northern (southern) cusp to north (south) under southward IMF conditions, while it extends from northern (southern) cusp to south (north) under northward IMF conditions.
closed1	Closed geomagnetic field lines in the nightside. Some of them may be the new closed field lines (see description of closed2) that have been convected to the nightside.
IMF2	Formed in the tail where one section is from an open1 field line, the other section is from an IMF1 field line or an open2 field line. It is detached from the magnetosphere and flows tailward away to become the IMF again.
open2	New open field line formed by one section from an IMF1 field line and another section from a geomagnetic field line. It drapes around the magnetopause and extends either from southern cusp to north or from northern cusp to south in the solar wind.
open3	New open field line formed when an IMF1 field line or an open2 field line reconnects with a closed1 field line, and this new open field line is in the nightside as a whole. It also extends either from southern cusp to north or from northern cusp to south.
closed2	New closed field line formed when an open2 field line reconnects with an open1 field line with footprint in the opposite hemisphere, or with a closed1 field line. It is formed in the dayside and is most likely convected around the magnetopause to the nightside.

[18] The simulation shows three topological types of magnetic field lines near the magnetopause: the first type is IMF field lines in the magnetosheath with both ends in the solar wind; second, open geomagnetic field lines with one end in the ionosphere and the other end in the solar wind; and third, closed geomagnetic field lines with both ends in the ionosphere. We classify the field lines according to their topology and formation characteristics. These classifications are listed in Table 1, and examples are shown in Figure 1.

[19] *Ogino et al.* [1994] found some similar magnetic field lines in their simulation of the response of the magnetosphere to a northward turning of the IMF. They classified the geomagnetic field lines into seven types from type "A" to type "G." Their "A," "B," and "C" type field lines seem to be the geomagnetic field lines when the IMF is still southward. The "D" type field lines are newly closed dayside field lines, and would be closed2 field lines according to our definition in Table 1. The "E" type field lines are closed field lines which have been convected from the dayside into the tail, and would be closed1 field lines that evolved from closed2 field lines. The "F" field lines are new IMF field lines formed by reconnection at high latitudes between IMF field lines and closed magnetospheric field lines in their simulation, and would be IMF2 field lines in our notation. The "G" type field lines are closed magnetospheric field lines about to undergo reconnection, and would be closed1 field lines in our notation as the one shown in Figure 1.

[20] With the classification in Table 1, we identify the possible reconnection processes near the magnetopause under northward IMF conditions as the six processes (a–f) listed in Table 2. Each process can occur at either the northern magnetosphere boundary or the southern boundary. At the beginning of the northward IMF conditions, the magnetosphere is open as a result of previous southward IMF conditions. There are only open1 field lines participating in high-latitude reconnection. The open1 field lines are eroded by the high-latitude reconnection. Reconnection processes a and d may then occur. The closed field lines (closed1) beneath the open1 field may then emerge and their participation in high-latitude reconnection becomes possible; thus the reconnection processes b and e may occur. Our simulation shows that these two processes can also occur after the newly created closed field lines have been convected to the nightside along the magnetopause, as indicated by the closed1 field line in Figure 1. The 2-D projection of field lines in Figure 1 seems to indicate that the open1 field will block the open3 field line and thus block processes c and f. Examining examples of closed1 and open3 field lines, we find that there are closed1 field lines whose

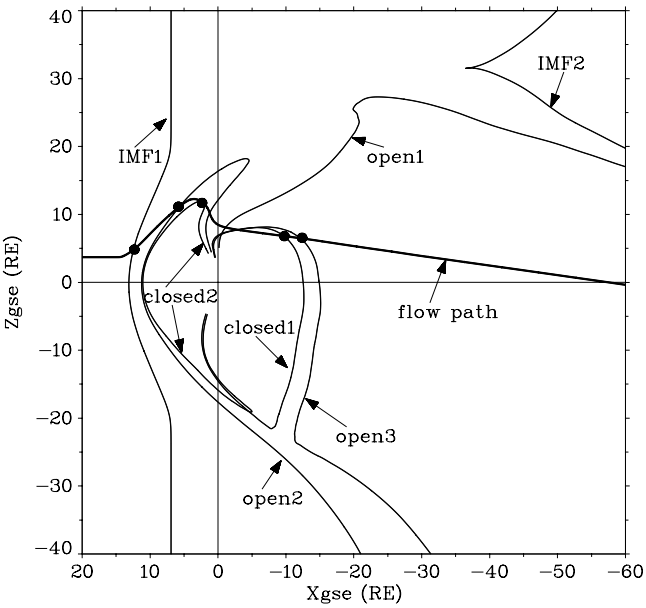

Figure 1. Possible topology of the magnetic field line threading a fluid element in the solar wind or the magnetosphere. This is also a sequence of FIMFL topology changes for a solar wind fluid element entering the magnetosphere and convecting tailward. The field lines and the flow path are projected on the GSE noon-midnight meridian. The thinner lines are the frozen-in magnetic field lines and the wider line is the path of the fluid element. The solid circles indicate the intersections between the path and the field lines. For the open1 and IMF2 lines, the intersections are in the far tail and are out of this figure's boundary.

Table 2. High-Latitude Reconnection (a–f) and Convection (g–i) Processes

Process	Relation
a	IMF1 + open1 → open2 + IMF2
b	IMF1 + closed1 → open2 + open3
c	IMF1 + open3 → open2 + IMF2
d	open2 + open1 → closed2 + IMF2
e	open2 + closed1 → closed2 + open3
f	open2 + open3 → closed2 + IMF2
g	open2 → open1
h	open3 → open1
i	closed2 → closed1

northern and southern sections both appear on the high-latitude magnetopause boundary. The resulting open3 field line thus may not be blocked by the open1 field. Therefore, reconnection processes c and f may occur in the opposite hemisphere to the one where the open3 field line is formed.

[21] When a solar wind plasma element flows around the magnetosphere, its FIMFL's topology may undergo a series of changes along the flow path at times when the FIMFL reconnects with another field line. Each topological change means that the fluid element enters into another topological region, i.e., crosses a separatrix. One example is shown in Figure 1, which displays the path of a solar wind fluid element that enters and leaves the magnetosphere and the FIMFL of the fluid element. The fluid element's FIMFL first changes from IMF1 to open2 as a result of reconnection process a, b, or c at the northern magnetosphere boundary. The fluid element thus flows from solar wind to the open region, which is the tail lobe or mantle. The FIMFL then changes from open2 to closed2 as a result of d, e, or f reconnection process at the southern magnetosphere boundary. At the closed2 stage, this fluid element has entered the dayside magnetosphere. The closed2 field line continues to convect tailward to the nightside and becomes a closed1 field line. It changes to open3 field line because of a reconnection process of b or e at the southern magnetopause boundary. The fluid element then becomes an element of the open region again. The open3 FIMFL, being pulled by the solar wind and stretched tailward, then becomes open1 after some time. Finally, the open1 FIMFL participates in another a or d reconnection process and creates an IMF2 field line. This fluid element is now detached from the magnetosphere and has merged with the solar wind again. We can summarize this sequence of field-line changes due to reconnection and convection as a sequence {*IMF1, open2, closed2, closed1, open3, open1, IMF2*} similar to the notation of mathematical permutations.

[22] Different flow paths may have different sequences of FIMFL topology changes. Identifying the sequence of topology changes of the FIMFL of a fluid element from the solar wind helps us study the transport of solar wind plasma into the magnetosphere. The reconnection processes listed in Table 2 allow us to identify all possible sequences. A fluid element on any one of the two flux tubes before reconnection (on the left side of the reconnection relation in Table 2) will become a fluid element of one of the two new flux tubes after reconnection (on the right side of the relation). One of the flux tubes in a relation's right side can possibly then become a flux tube in another relation's left side. In addition, the open2 and open3 field lines can become open1 field lines, and closed2 field lines can become closed1 field lines as a result of convection. Listing all the possible combinations of the reconnection relations, we can then find all the possible sequences. To complete this scheme, we add three more convection relations to describe in Table 2 the changes of the magnetic field line in shape and position due to convection.

[23] To describe a sequence of a changing FIMFL topology, we use the magnetic field-line types defined in Table 1 to construct a sequence set. Obviously, the first element of a sequence set is always IMF1, since the fluid element flows from solar wind. IMF2 may be the final element of a sequence set since it never appears in the left side of a relation. An IMF2 field line is a detached magnetospheric field line. Closed1, closed2, and open1 can also be a final element of a sequence because they may not change any more, at least until the end of a fluid element tracing period. In our analysis, we set the tracing period to be 90 min. In other words, the sum of the total time iteration steps is 90 min. On the basis of our simulation results, this time period is the typical time scale for a fluid element to enter the near magnetotail region.

[24] Using the method described above, a large number of sequences are possible. However, in reality, most of them will never occur. It is because the reconnection relations in Table 2 do not discriminate which section of one flux tube will reconnect with which section of the other flux tube, and they also do not discriminate the reconnection location (north or south cusp). Thus, many combinations of the FIMFL types in a sequence set are not physically possible, or are unlikely to occur. Table 3 lists the sequences that we have observed in our simulations.

[25] Of these sequences, we are mainly interested in the cases of 5, 6, 7, and 8 because only in these sequences will the FIMFL ever be closed for some time along the flow path of a fluid element. These sequences represent the possible paths of a fluid element on the IMF field-line section draping on the dayside magnetopause near the Sun-Earth line, which is eventually cut from the IMF flux tube by the double high-latitude reconnection. Such fluid elements from the solar wind are considered as captured by double high-latitude reconnection. Other sequences represent the paths of the fluid elements that will not enter the magnetosphere. Such fluid elements are from the northern end or southern

Table 3. Common Sequences of FIMFL Topological Changes Along a Flow Path

ID	Sequence
1	{*IMF1*}
2	{*IMF1, IMF2*}
3	{*IMF1, open2, IMF2*}
4	{*IMF1, open2, open1, IMF2*}
5	{*IMF1, open2, closed2*}
6	{*IMF1, open2, closed2, closed1*}
7	{*IMF1, open2, closed2, closed1, open3, open1, IMF2*}
8	{*IMF1, open2, closed2, closed1, open3, IMF2*}
9	{*IMF1, open2, open3, open1, IMF2*}
10	{*IMF1, open2, open3, IMF2*}
11	{*IMF1, open3, IMF2*}
12	{*IMF1, open3, open1, IMF2*}

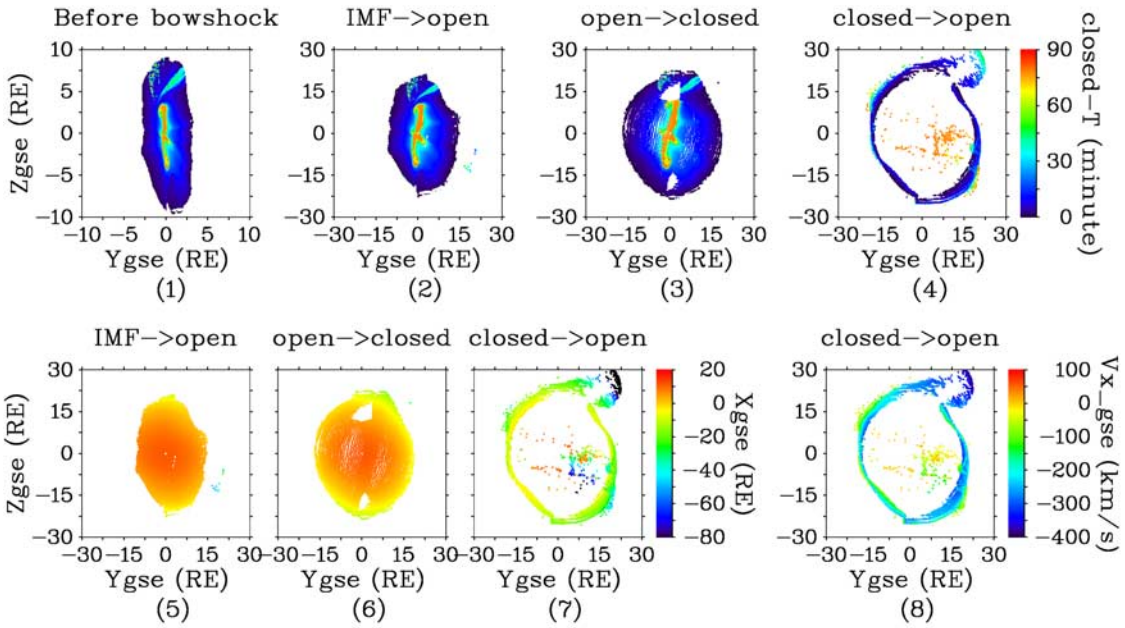

Figure 2. Solar wind entry window at different stages. The IMF is pure northward and the geomagnetic dipole tilt is zero. Frames 1–4 show the color-coded closed time, which is the life time of a newly created closed field line during a flow path tracing. Frames 5–7 show the color-coded X_{gse} coordinate corresponding to Frames 2–4, respectively. Frame 8 shows the color-coded average V_x corresponding to Frames 4 and 7. See text for detail description.

end section of an IMF flux tube that is cut from the IMF flux tube by high-latitude reconnection.

[26] In cases 5 and 6, the newly created closed field lines become part of the geomagnetic closed field, at least until the end of the tracing period. For cases 7 and 8, the fluid element is first captured by double high-latitude reconnection, and then is released by another double high-latitude reconnection event occurring at the same locations as the previous one. Thus, a captured solar wind fluid element will either become the plasma of the magnetosphere, or will eventually be released toward the far magnetotail and detached from the magnetosphere.

4. Solar Wind Plasma Entry

[27] We study the solar wind flow and its FIMFLs by tracing a uniformly distributed array of 400 × 400 fluid elements, starting from a plane upstream of the bowshock at X_{gse} = 20 R_E with Y_{gse} and Z_{gse} ranging from −20 R_E to 20 R_E. When tracing a fluid element, we derive its FIMFL for each computing step and determine its topology (IMF, open, or closed). The field line topology is determined by finding out where the end points of the computed field line locate. A field line with both end points within 6 R_E is considered to be a closed geomagnetic field line. It is considered to be an open field line if only one end point is within 6 R_E. Otherwise, the field line is considered to be an interplanetary magnetic field line.

4.1. Entry Window

[28] We consider a fluid element as being captured if its FIMFL ever becomes closed for some time (hereafter called closed-time) along the flow path, as described by the sequences 5, 6, 7, and 8 in Table 3. Closed-time is related to the entry position. Entering at the subsolar point (y = 0, z = 0), the fluid element's closed time is long, at least 30 min. Entering at a point away from the subsolar point, the fluid element's closed time may be only minutes or less than 1 min. In other words, it quickly enters and exits the magnetosphere.

[29] In frames 1–4 of Figure 2, we plot the GSE YZ plane projection of each captured fluid element at four stages: (1) when the fluid element is launched from a location before the bowshock; (2) when the FIMFL of the fluid element changes from IMF to open, usually at the dayside magnetopause; (3) when the FIMFL changes from open to closed, also usually at the dayside magnetopause; and (4) when it changes from closed to open again, usually in the tail or when the tracing is ended. In these four plots, color is used to indicate which flow element is captured and its duration in a closed field topology. Thus, any color other than white indicates that the fluid element is located on a closed field line for at least a short period of time. For the color points on the plots of the four stages as shown in frames 1–4 in Figure 2, each point of the same color at one stage has a one-to-one correspondence to the same color domain on the other three frames with the flow path passing through them (see Figure 1). Under constant boundary conditions within a certain time period, the plasma flow in and out of the magnetosphere will be relatively stable. We can think of the color areas on the plots of the first three stages as solar wind "entry windows" at three different stages. The solar wind plasma enters the magnetosphere through these windows.

[30] We also indicate the X_{gse} coordinate of each fluid element for the corresponding stages as shown in frames

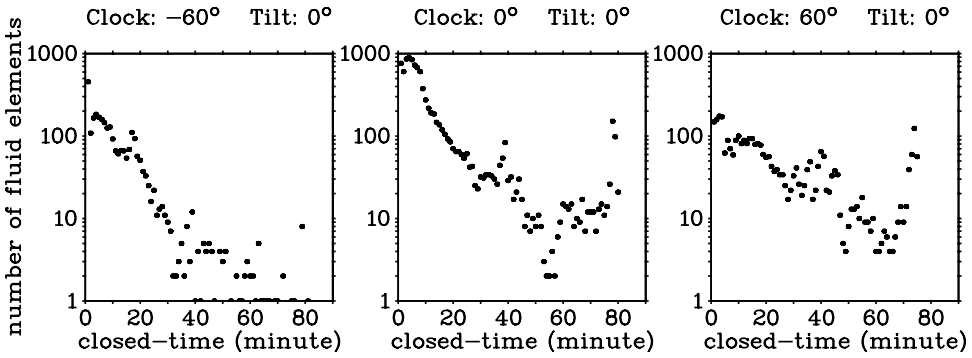

Figure 3. Examples of distribution of the time period (closed time) that a fluid element dwells on closed field line. The left is closed time distribution for IMF with −60° clock angle. The middle is for pure northward IMF, and the right is for 60° IMF clock angle. All have zero geomagnetic dipole tilt. These three distributions all have peaks around 5 min, 40 min, and 80 min.

5–7 in Figure 2. Note that the corresponding times for each location of these fluid elements may not occur at the same time for stages 2, 3, and 4. In other words, the fluid elements passing through the entry window at stage (1) simultaniously may arrive at other stages at different times. The plots in frames 5–6 of Figure 2 represent a three-dimensional view of the entry windows at the magnetopause. By plotting the magnetopause location where the ions entered the magnetosphere, *Walker et al.* [2003] created an entry area similar to the one in frame 6 of Figure 2 from ion trajectory calculations. *Peroomian* [2003b, 2003a] also created plots similar to the one in frame 1 of Figure 2 by showing launching positions of particles that reach the magnetopause.

[31] Obviously, the entry window has a different shape at different stages. Our analysis also shows that for each stage, different fluid element launching times may result in somewhat different shapes of the entry windows as well. The entry widow with launching times near the turning of southward IMF to northward IMF is different from the ones with launching times several hours after the northward turning of the IMF. Even after hours of constant uniform solar wind and IMF input conditions, the shape of entry window is not perfectly symmetric and still changes in time. This change occurs when the reconnection rate is not constant as a result of the anomalous resistivity, current density variations, and the dynamic nature of the plasma flows. The ionosphere variations also cause the entry window to change in time and break its symmetry (see section 5.6). The shape of entry regions shown by *Peroomian* [2003b, 2003a] also shows some irregular features, which the author attributes to nonadiabatic acceleration of ions at the reconnection sites, acceleration of ions in the MP current layer, and the direction of interplanetary electric field.

[32] The plasma fluid elements on the same captured flux tube should in principle flow to the same area and have the same amount of closed-time, if the assumption of frozen-in flux tube holds. However, on the entry window near the end of the north or south boundary, the fluid element has a shorter closed time than the one in the center and flows to a different area. Examining the FIMFLs of fluid elements on the same starting IMF flux tube, we find that the plasma element near the reconnection site jumps from the original flux tube to another flux tube. This movement results from the fact that the frozen-in condition is broken at the reconnection site, where the plasma is decelerated or accelerated. Indeed, we find that the electric field and current density are high in this area, although not shown here.

[33] The time between stage 2 and stage 3, i.e., the time between a field line's reconnecting in one hemisphere and then reconnecting in the other hemisphere, is short, from seconds to minutes. The entry window of stage 3 shown in frame 6 of Figure 2 can be considered as the separatrix surface, inside which there is a layer of newly created closed field lines. Outside this separatrix surface, there is a layer of open field lines. The white regions within the entry windows in frames 3 and 6 correspond to the two cusps. The high-latitude reconnection occurs tailward of the cusps, and thus the entry windows at stage 2 and stage 3 on the dayside magnetopause should cover the cusps. However, the captured fluid elements entering at a position near the cusp do not flow along the newly closed field lines into the cusps. Instead, they convect along the magnetopause toward the nightside. Consequently, two white regions corresponding to the two cusps appear on the entry window on the dayside magnetopause at stage 2 and stage 3.

4.2. Solar Wind Entry Flow Pattern

[34] Frames 1–4 in Figure 2 indicate that the captured plasma fluid elements may be classified into groups according to their closed time values. The closed time is longest for fluid elements entering near the center of the entry window and is shortest for fluid elements entering near the boundary of the entry window. Figure 3 gives examples of closed time distributions for different IMF clock angles. The distributions show a very high peak for a closed time less than 20 min. There is another peak at around 70 to 80 min, which is most obvious for 0° and 60° IMF clock angles. There is also a small peak at around 40 min. We may approximately define the three groups with the closed time domains [60,90], [30,60) and (0,30) as A, B, and C, respectively. Note that the total tracing time is 90 min in our analysis, and there is a travel time of about 10 min for the fluid elements to reach the magnetopause.

[35] Frames 4 and 7 in Figure 2 show the distribution of the entered plasma at their last stage of being in closed field and thus can reveal some information about the destination and convection path of the captured plasma.

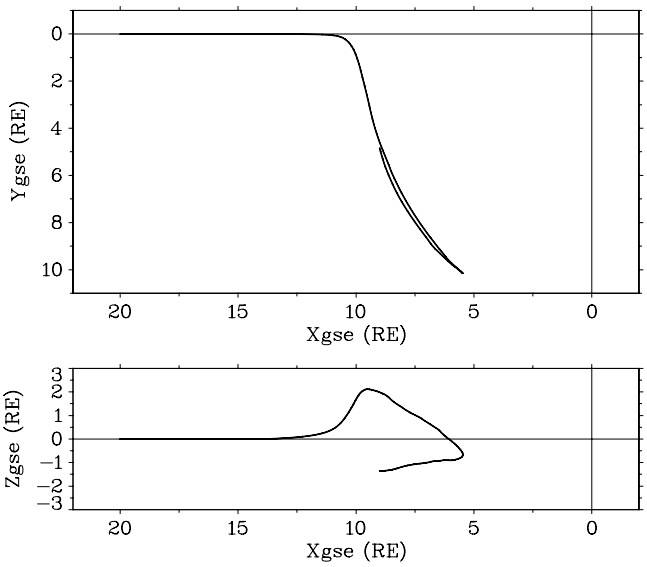

Figure 4. GSE XY plane and XZ plane projection of the flow path of a fluid element that enters the dayside magnetosphere and stays there.

[36] The fluid elements of group A are located on the central flux tubes that face the nose of the magnetopause and are the brightest points on the entry window. The FIMFLs of these fluid elements stay for a long period of time in closed topology, usually more than 60 min. This group is also divided into two subgroups. The fluid elements of one subgroup, called group A1 here, flow to near the dawnside or duskside of the plasma sheet, and some can flow deep into the plasma sheet. Their flow speed is low, usually less than 100 km/s. Examining the density and temperature along the flow paths of some of these fluid elements, we find that the density is $\sim$1–10 cm^{-3}, and the temperature is about 1 keV when they are in the plasma sheet. Comparing these values to the properties of the observed cold dense plasma sheet [e.g., *Fujimoto et al.*, 1996, 1998; *Phan et al.*, 1998; *Fuselier et al.*, 1999; *Øieroset et al.*, 2002], we conclude that this subgroup of solar wind plasma elements may be viewed as the main component of what is called the CDPS from observations. The other subgroup of fluid elements, called group A2 here, is represented by the points with long closed-time in frame 4 and positive X_{gse} coordinates in frame 7 of Figure 2. This subgroup of fluid elements flows into the dayside closed field region, and their associated new closed field lines become part of the closed field lines in the dayside. Figure 4 shows a flow path of such fluid elements. The sequence of its FIMFL change (not shown here) along the path is also an example of the sequence 5 in Table 3. This fluid element flows from a place near the Sun-Earth axis to the magnetosphere. After its FIMFL becomes closed, i.e., closed2 field line, the fluid element first flows duskward along the magnetopause and then turns south and dawnward. The flow speed in the magnetosphere is very slow since the whole path takes 90 min.

[37] The fluid elements of group B enter through positions around the group A fluid elements, and are represented by the green or blue points (grey points for black-and-white version of the figure) on the entry windows shown in frames (1)–(3) of Figure 2. Their closed topology time period is shorter than group A fluid elements and ranges from about 30 to about 60 min. Frame 4 of Figure 2 indicates that most of these fluid elements flow to the boundary of the magnetotail, creating a dawn/dusk asymmetric feature. The dawnside fluid elements of this group flow northward and tailward along the magnetopause, whereas the duskside fluid elements flow southward and tailward along the magnetopause. The group A1 fluid elements also have a similar, but less obvious, asymmetric feature as group B fluid elements.

[38] The fluid elements of group C are represented by the points with dark blue color on the entry windows in Figure 2. They flow all over the magnetopause boundary. Most of them have closed time of less than 10 min and stay in the closed field in the very near tail where X_{gse} is greater than ~ -10 R_E. The fluid elements of group C, together with those of group B, form a closed boundary layer in the near magnetotail. The plasma flow of group C has the fastest flow speed among the three groups, while the group A fluid elements have the slowest speed, as indicated by the average V_X during the closed-time period in frame 8 of Figure 2.

[39] Occasionally, some of the group C fluid elements passing near the reconnection region, as shown in the light blue stripe at northern duskside of the entry windows in frames 1, 2, and 3 of Figure 2, may jump from original flux tubes to flux tubes with longer closed-time and faster convection speed. At stage 4, these fluid elements flow to the far tail (40–80 R_E) with their y and z projections becoming larger than the other fluid elements, and thus form a bulge shown in the frames 4, 7, and 8 of Figure 2. However, of all the entry windows that we have computed for various geospace conditions and different fluid-element-launching times, this feature appears in just a few of them. We have not found a significant relation between this feature and any particular geospace conditions. For simulations with constant ionosphere conductance, the entry window is symmetric and does not have this bulge (see section 5.6). It is possible that the interaction between the ionosphere and the outer magnetosphere creates some fluctuations during the convection of flux tubes near the magnetopause, which cause this feature.

[40] The above classifications and descriptions are based on a simulation with pure northward IMF, zero geomagnetic dipole tilt angle, and average solar wind conditions. However, the classification of three groups of entry fluid elements holds for all other solar wind and IMF conditions, as will be shown in section 5. A survey of entry windows, as the one shown in Figure 2, for various IMF magnitude and solar wind conditions but with pure northward IMF and zero dipole tilt angle, shows that their flow pattern and distribution of the flow elements are all similar. The classification of the three groups of captured flow elements is applicable for all conditions that we have studied. The formation of the three groups of captured plasma (or new-closed field lines) is mainly due to the entry position of the fluid elements. However, the $\mathbf{J} \times \mathbf{B}$ force on the new-closed field lines and the electrodynamic properties of the magnetopause may also affect such group classification.

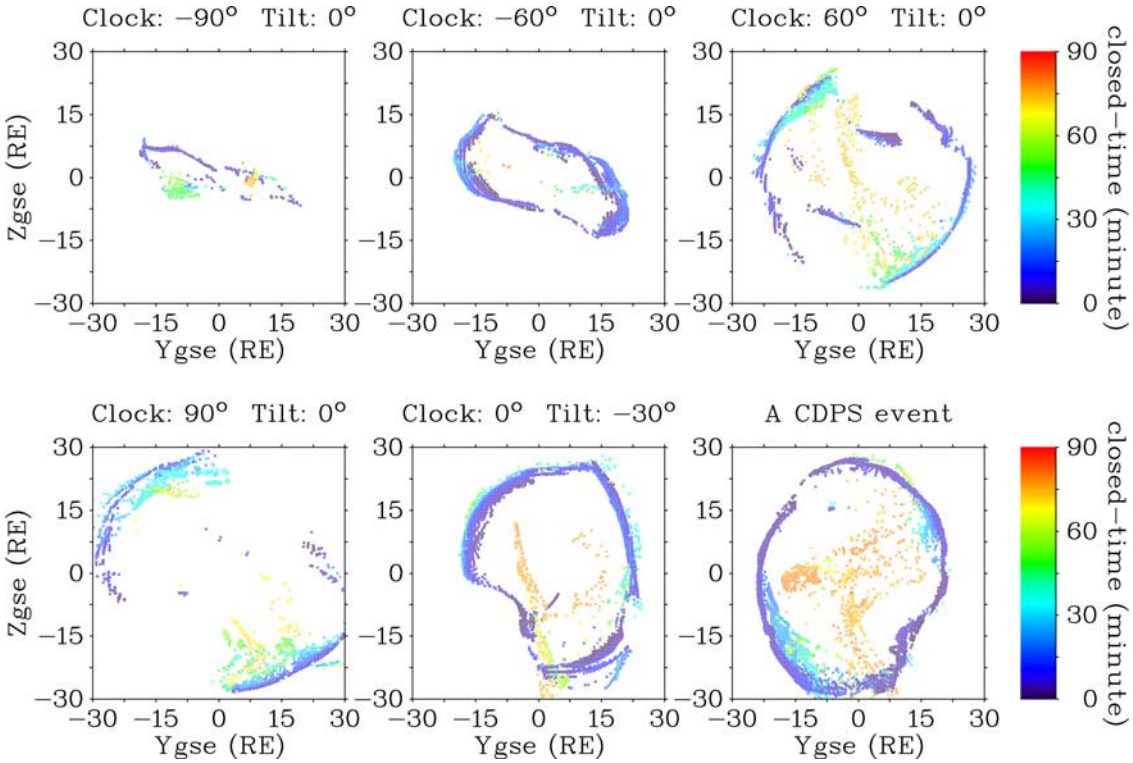

Figure 5. YZ(GSE) plane projection of captured fluid elements at the stage when their frozen-in magnetic field lines change from closed field lines to open field lines or when the tracing of the fluid elements ends. These plots are the same kind of plot as in frame 4 of Figure 2, but for different IMF clock angles and dipole tilt angles, as well as for the CDPS event on 23 October 2003, where the IMF is almost pure northward.

[41] In our simulations, the three groups of captured fluid elements go to distinctive regions in the tail, as discussed above. We further investigate how the geospace conditions affect the convection and destination of the captured plasma.

[42] Figure 5 shows plots in the same manner as frame 4 of Figure 2 for other IMF clock angle and dipole tilt angle cases. These plots reveal some information about the destination and convection path of the captured plasma for various IMF clock angles and dipole tilt angles. Group A fluid elements flow to locations well inside the magnetosphere. Group B and group C fluid elements seem to flow along the magnetopause. For cases of negative IMF clock angles, the amount of captured plasma seems to be less than the amount for cases of positive IMF clock angles. This asymmetry will be discussed further in section 5.6. Comparing frame 4 of Figure 2 with the plot with title "A CDPS event" in Figure 5, we find that the distribution of group A and group B fluid elements are much different in these two plots. In the simulation for Figure 2, the IMF is pure northward and its strength and the solar wind conditions are constant. In the simulation of the CDPS event, the IMF is also near due northward, but its strength and the solar wind conditions are not constant. Therefore, the flow pattern may also be affected by IMF strength and solar wind conditions.

[43] The boundary layer formed by newly created open field lines also affects the flow behavior of the captured fluid elements. In other words, it affects the convection of the newly created closed field lines. All the open field lines created by high-latitude reconnection extend either from the northern cusp to the southern hemisphere in the solar wind, or from the southern cusp to the northern hemisphere in the solar wind, as shown in Figure 6. Draping over the magnetopause, such open field lines may have a curvature force on the magnetopause in the regions where there is curvature in the magnetic field. The direction of this curvature force depends on how the open field lines extend from the cusps. Such curvature force may affect the convection of the new-closed field lines. When the open field lines on the duskside and dawnside extend in the opposite direction, as shown in the top two rows of frames in Figure 6, the open field lines may exert a torque over the magnetopause.

[44] We also found that the ionosphere has a significant effect on the convection of the new-closed field lines. We will discuss this in section 5.6. The convection behavior of the new-closed field lines is related to the entry rate (see section 5.5). Such convection is affected by IMF clock angle, dipole tilt angle, solar wind conditions, new-open field lines as discussed above, and the ionosphere. However, a detailed study of the convection of new-closed field lines in the tail, as well as of the formation of the three groups of captured fluid elements, is beyond the scope of this paper. The main purpose of Figure 5 is to show that the captured plasma can flow well inside the magnetosphere besides along the magnetopause.

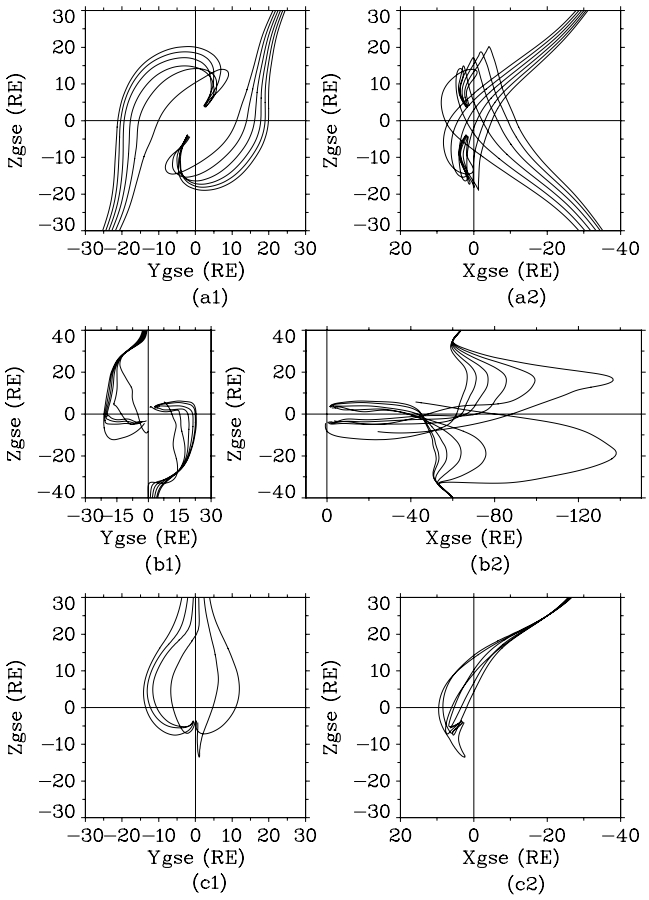

Figure 6. Examples of newly created open field lines as a result of high-latitude reconnection. The field lines are projected onto the GSE YZ plane and XZ plane. The field lines in frames a1 and a2 are examples of open2 field line and are computed from the simulation with 30° IMF clock angle and zero geomagnetic dipole tilt. The field lines in frames b1 and b2 are examples of open3 field line and are computed from the simulation with pure northward IMF and dipole. The field lines in frames c1 and c2 are examples of open2 field line and are computed from the simulation with pure northward IMF and −30° dipole tilt.

4.3. Distribution of Cold Dense Plasma

[45] We have so far discussed the distribution and convection behavior of the captured solar wind plasma. We also classified the captured solar wind flow elements into three distinct groups. Since the captured plasma is magnetosheath plasma, which is cold (<1 keV) and dense (>1 cm^{-3}) compared to typical plasma sheet plasma (1–10 keV, ∼0.3 cm^{-3}), despite a slightly heated component that comes from high-latitude reconnection, the distribution of the captured plasma represents the distribution of cold dense plasma in the magnetosphere. Here we assume that double high-latitude reconnection is the dominant process that brings the magnetosheath plasma into the magnetosphere because our simulation reproduces the observed cold dense plasma sheet and its typical properties [*Øieroset et al.*, 2005; *Li et al.*, 2005]. However, we also note that our simulations do not have sufficient resolution to resolve the Kelvin-Helmholtz instability, which is considered to be another important process that possibly transports solar wind plasma into the magnetosphere.

[46] The observations show that a cold dense plasma sheet is often observed in the midtail after a period when the IMF has been northward, on average, for several hours [*Terasawa et al.*, 1997; *Fujimoto et al.*, 1998; *Phan et al.*, 1998, 2000]. Most of the time, the CDPS is found to be located near the flanks and sometimes found to penetrate to the center of the tail [*Fujimoto et al.*, 2002]. It is also often found at high magnetic latitudes ($|B_x| > 15$ nT) in the plasma sheet [*Phan et al.*, 1998; *Øieroset et al.*, 2002]. The CDPS plasma is characterized by higher density (∼1 cm^{-3}), lower temperature (<1 keV), and small flow velocity (<100 km/s), compared to the usual hot (>1 keV) and tenuous (∼0.1 cm^{-3}) plasma sheet. It is found to be located on closed field lines [*Fujimoto et al.*, 1998]. Comparing the flow paths and properties of the fluid elements of group A1 (Figures 2 and 5) with observed properties of the cold dense plasma sheet, we conclude that they form the main component of the observed cold dense plasma sheet. They flow along the dayside magnetopause and enter mostly into a region near the flanks in the near tail.

[47] Figures 2 and 5 suggest that the other groups form a boundary layer with closed field topology from the dayside magnetopause to the near-tail magnetopause. In the simulation, the plasma in this closed boundary layer has density (∼2–4 cm^{-3}) and temperature (∼0.3–1 keV) that are intermediate between those in the magnetosheath and the plasma sheet.

[48] We can also infer from frame 2 of Figure 2 and Figure 6 that there is a boundary layer with open field topology between the magnetosheath and the closed boundary layer or between the magnetosheath and the lobe field beyond the closed boundary layer under northward IMF conditions. The properties of the plasma in this layer are also intermediate between those in the magnetosheath and the plasma sheet.

4.4. Depletion of Cold Dense Plasma and Geomagnetic Field Convection Cycle

[49] Under constant northward IMF conditions, high-latitude reconnection continuously occurs between the IMF and the high-latitude geomagnetic field tailward of the cusp, and consequently causes magnetosheath plasma to enter the magnetosphere constantly. Two questions arise: (1) Does the lobe field vanish at some point and the whole magnetosphere becomes completely closed? And (2) does the density of the plasma sheet increase up to magnetosheath values? These are not what we have observed in our simulation. Observationally, it is known that the polar cap size shrinks substantially under sustained northward IMF but that it never totally disappears [*Milan et al.*, 2004]. Cluster observations during the steady long period of northward IMF on 23 October 2003 UT show that the density of CDPS first rises over a 3-h period and then remains at the 1.5 cm^{-3} level during nearly the rest of the period of ∼30 h [*Øieroset et al.*, 2005]. Our simulation of this event also shows a nearly constant density of the CDPS after about 3 h of northward IMF [*Li et al.*, 2005]. Thus, there must be a process that depletes the cold dense plasma

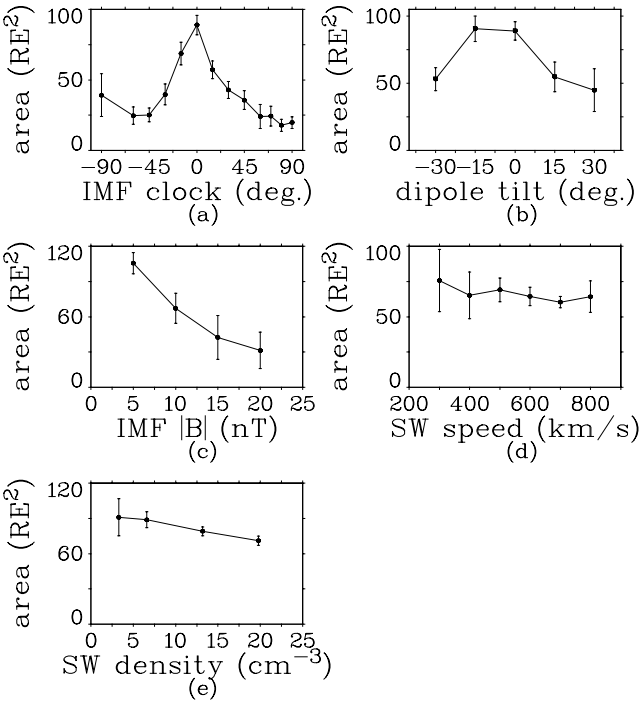

Figure 7. Variation of entry window's area which includes all the captured fluid elements. Each data point is an average of nine entry windows computed for nine different fluid element launching times. The error bar indicates the standard deviation of the variation of these nine entry widows.

so that a balance between plasma inflow and outflow can be established.

[50] The reconnection processes b and e discussed in section 3 indicate that the magnetosphere will never completely close since new open field lines, open3 field lines, are created from closed field lines for purely northward steady IMF. Such processes also provide the cold dense plasma depletion mechanism. After the reconnection processes b and e occur, some closed1 field lines, the newly created closed field lines that have been convected to the tail, become open again. The sequences 7, together with Figure 1, and 8 discussed in section 3, show a process that releases the captured cold dense plasma by subsequent double high-latitude reconnection at the same locations as those where the dayside plasma is being captured simultaneously. A plasma fluid element that has been captured may become one element on a new IMF field line that will flow away from the magnetosphere. Diffusive processes may also let the cold dense plasma move into neighboring regions, such as the inner magnetosphere and the lobes. It is also possible that some cold dense plasma depletes into the ionosphere along closed flux tubes. However, the simulation results indicate that the re-reconnection process is sufficient to drain away enough cold dense plasma from the plasma sheet to establish an equilibrium of inflowing and outflowing plasma.

[51] Figure 5 shows the y and z GSE coordinates of the captured fluid elements in the tail when the associated new-closed field lines change to open. The y and z coordinates and the associated color show that it takes $\sim$1–$\sim$80 minutes for a new-closed field line to convect to a place where it becomes open, depending on the entry window location of the corresponding fluid element. Some new-closed field lines that stay closed at the end of the tracing will also open eventually if we extend the tracing time. Thus most of the entering solar wind plasma may eventually exit the magnetosphere under a steady northward IMF.

[52] Figure 1 and the sequences 7 and 8 also indicate a cycle of geomagnetic field line convection for northward IMF conditions. Considering a field line in the tailward northern cusp, it goes from open1 (or closed1), becomes open2 convecting sunward, then becomes closed2 convecting tailward, continues to become closed1, and may finally change to open1. The convection in the ionosphere associated with high-latitude reconnection has been observed and studied theoretically [e.g., *Maezawa*, 1976; *Reiff and Burch*, 1985; *Crooker*, 1992; *Crooker et al.*, 1998; *Knipp*, 1993]. A signature of this convection cycle was recently observed by SuperDARN in the dayside portion of the open/closed field line boundary in the ionosphere [*Imber et al.*, 2006].

5. Entry Window Dependence on Solar Wind, IMF, and Geomagnetic Dipole Tilt

[53] In the present study, we have established the entry window through which the solar wind plasma will be on closed field for a certain time period due to the double high-latitude reconnection process. The shape and size of the entry window is expected to be controlled by the characteristics of the geomagnetic field, the solar wind, and IMF.

[54] We now compute the entry windows from simulations for various geospace parameters. The dependence of the area of the entry window on the geospace parameters is summarized in Figure 7. Since the entry window changes in time slightly even under constant solar wind and IMF conditions, we compute the entry windows for different fluid element launching times and compare their average and standard deviation in Figure 7. For each data point in Figure 7, there are nine computed entry windows corresponding to fluid element launching times 0455, 0500, 0505, 0555, 0600, 0605, 0655, 0700, and 0705, where 0455 means 4 h and 55 min after the beginning of a simulation. We emphasize that the northward IMF turning was set to occur at 0300 at the magnetopause after the simulations were initiated.

5.1. IMF Clock Angle Dependence

[55] Figures 7a and 8 show how the area of the entry window and its orientation change with the IMF clock angle. The size of the entry window is determined by all the fluid elements with nonzero closed time. The window size becomes smaller when the absolute value of the clock angle is larger and the window orientation aligns with the IMF direction. However, the area of the entry window for IMF with pure dawn-dusk direction is still significant, instead of its decreasing to zero. The distribution of the window area is rather symmetric with respect to a pure north direction. The particle entry region shown by *Peroomian* [2003a] is also aligned with the IMF direction in the YZ plane and has a significant entry area for westward IMF.

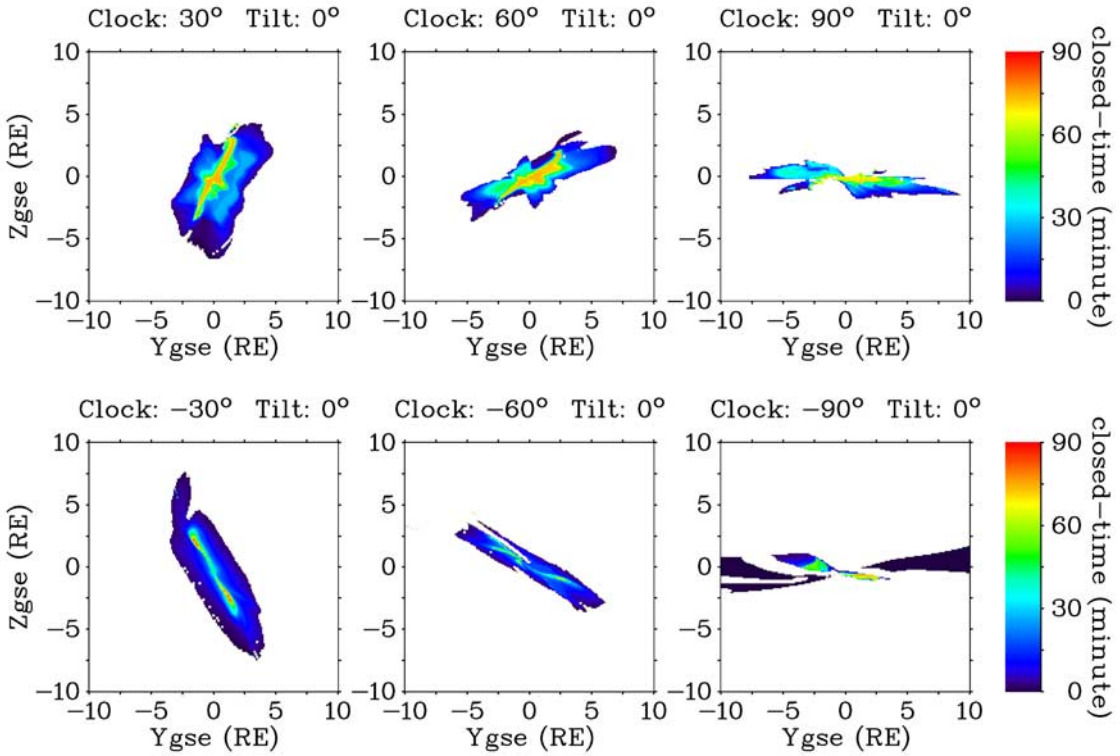

Figure 8. Solar wind entry windows located before the bowshock for different IMF clock angles. The geomagnetic dipole tilt is zero, and the solar wind conditions have the normal values. They are the same kind of plot as the one in frame 1 of Figure 2.

[56] In our simulation, we find that the IMF clock angle may change when the IMF field line approaches the magnetopause before reconnecting with geomagnetic field line. The IMF field-line section draping around the magnetopause is deformed and tilted by the $\mathbf{J} \times \mathbf{B}$ force. For the IMF with near positive 90 degree clock angle, such deformation helps it become antiparallel to the southern dawn and northern dusk geomagnetic field lines and makes double high-latitude reconnection possible to create new closed2 field lines. For a negative 90 degree IMF clock angle, the IMF is deformed so that it becomes nearly antiparallel with the northern dawn and southern dusk geomagnetic field lines. As shown in Figure 9, a dawn-dusk field line near the subsolar point has a northward and duskward $\mathbf{J} \times \mathbf{B}$ force on the duskside of the boundary and has a northward and duskward $\mathbf{J} \times \mathbf{B}$ force on dawnside of the boundary. The force along the field line has the shape of a sine curve with the maximum about 6 R_E away from the subsolar point. Such a distribution of the $\mathbf{J} \times \mathbf{B}$ force makes this field line become antiparallel to a southern dawn or a northern dusk geomagnetic field at some point. Our simulation suggests that the IMF flux tube will be deformed in a certain direction depending on its location relative to the magnetopause subsolar point.

[57] In the simulations, we found that the IMF draping over the magnetopause can reconnect with open or closed field lines over a broad range of local time tailward of the cusp. Here, high-latitude reconnection may not be an strictly correct term, since reconnection can possibly occur near the dawn and dusk tail flanks. A better term may be tailward-of-the-cusp reconnection. *Nishikawa* [1998] also found reconnection at both the dawnside and duskside during northward IMF condition in his simulation using a three-dimensional electromagnetic particle code.

[58] In addition to the reconnection due to the antiparallel IMF and geomagnetic field at the reconnection location, component reconnection, in which shear angles between the magnetospheric field and the IMF can be much less than 180°, may also occur at the dayside magnetopause [*Sonnerup*, 1974; *Fuselier et al.*, 1997, 2000; *Chandler et al.*, 1999; *Trattner et al.*, 2004; *Bobra et al.*, 2004]. For component reconnection, there is an upper limit of the shear angle for a certain ratio of the field strength on both sides of the magnetopause [*Sonnerup*, 1974]. Since we have not investigated the reconnection location and the shear angles in detail, we cannot discriminate component reconnection and antiparallel reconnection in the simulation.

[59] During a double tailward-of-the-cusp reconnection process, generally, an IMF field line first reconnects with a magnetospheric field line at one side of the noon-midnight meridian in one hemisphere then at the other side in the other hemisphere. The two merging field lines having an upper limit of the shear angle and the geometry of the field lines near the cusps constrain the places where reconnection can occur, thus constraining the window size according to the IMF clock angle and determining the orientation of the window.

5.2. Geomagnetic Dipole Tilt Angle Dependence

[60] Figure 10 and frame b of Figure 7 suggest that a small negative (antisunward) dipole tilt angle between 0° and −15° maximizes the entry window. More solar wind

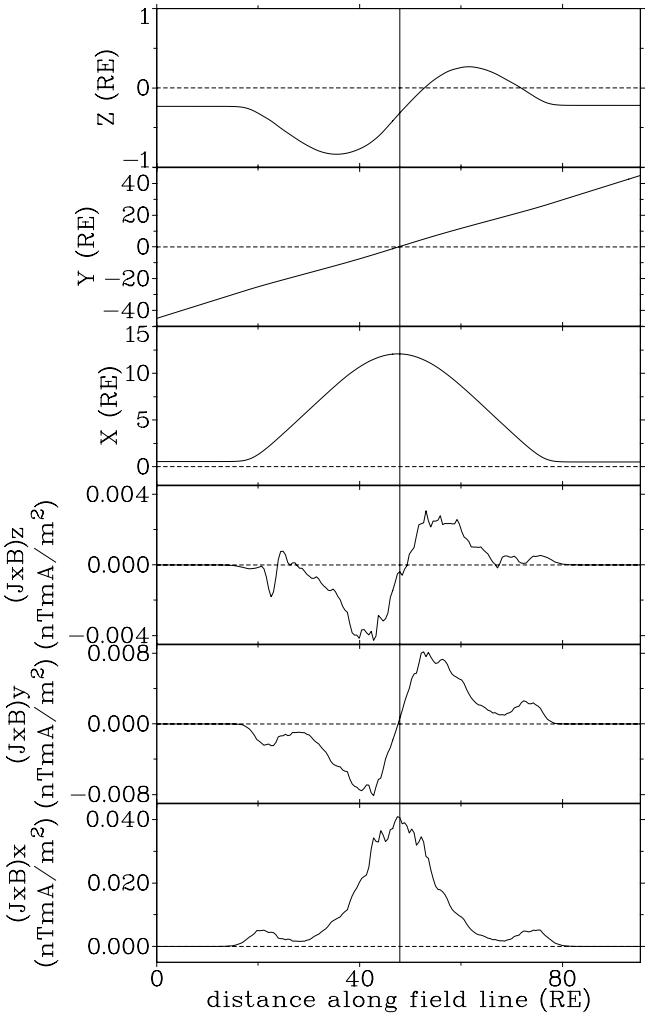

Figure 9. A snapshot of the **J × B** force distribution along a dawn-dusk magnetosheath magnetic flux tube from dawn to dusk looking from the Sun. The vertical solid line near the center indicates the subsolar point.

plasma is captured south (north) of the equatorial plane for positive (negative) tilt angle. Our preliminary study suggests that the convection behavior of the new-closed field lines may cause such entry characteristics. Our simulation shows that a new-closed field line with its northern (or southern) part near the high-latitude magnetopause in the tail will easily participate the high-latitude reconnection again and become open, as indicated by Figure 1, which shows that the closed1 field line changes to an open3 field line. When the geomagnetic dipole has a certain antisunward tilt angle, the northern and southern parts of a new-closed field line are not likely near the high-latitude magnetopause. It then is less likely to participate in another high-latitude reconnection, and thus is more likely to convect into the magnetosphere.

[61] Our simulations indicate that when the dipole tilt angle is positive, an IMF flux tube first interconnects with a geomagnetic field flux tube at the northern cusp and later at the southern cusp. This event is expected since an IMF flux tube with zero B_x will contact the northern cusp field first when the dipole tilts sunward. Note that the initial IMF B_x is set to be zero in our simulations. The opposite sequence holds for negative dipole tilt angles. Most of the open2 field lines will consequently have footprints in the northern hemisphere for positive dipole tilt angle. Examining the FIMFLs along some flow paths moving through the entry window for our simulations with dipole tilt angles of 15° and 30°, we find that all the FIMFLs become open with footprints in the northern hemisphere. Conversely, the FIMFLs become open with footprints in the southern hemisphere for tilt angles of −15° and −30°, as shown in frames c1 and c2 in Figure 6.

5.3. IMF Magnitude Dependence

[62] The entry window becomes thinner in the GSE y direction, and its area consequently becomes smaller when the IMF is stronger, as shown in Figures 7c and 11. The size of the magnetosphere becomes smaller in the GSE y direction as the IMF is stronger, which is indicated by the distribution of the captured plasma in the tail shown in Figure 12. In that figure, the B–C group fluid elements approximately show the size of the magnetopause in the tail for cases of low (5 nT) and high (20 nT) IMF magnitude. As the magnitude of the IMF increases, the magnetic pressure in the magnetosheath increases. Therefore, the size of the magnetosphere decreases slightly, and the magnetotail flaring angle also decreases slightly [*Petrinec and Russell*, 1996], since the contribution of magnetic pressure is small compared to the solar wind dynamic pressure effect in the simulations. In addition, as the IMF flux tubes drape around both the dawnside and duskside of the magnetotail from south to north, they exert a magnetic curvature force onto the magnetopause and squeeze the magnetotail from the dawnside and duskside. A stronger IMF leads to a stronger

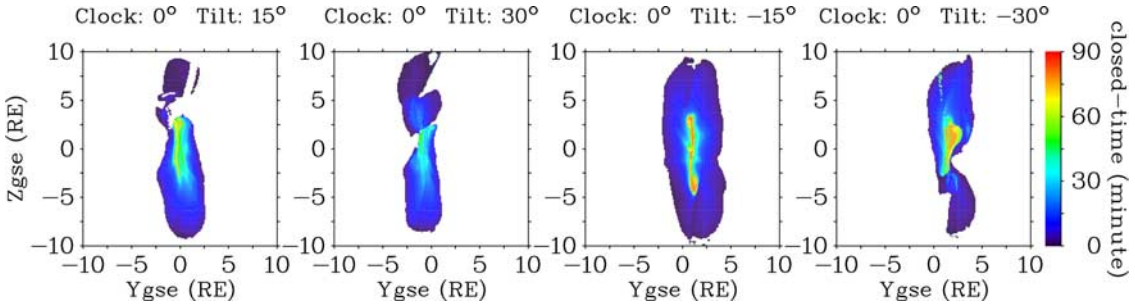

Figure 10. Solar wind entry windows located before the bowshock for different geomagnetic dipole tilt angles. The IMF is pure northward, and the solar wind conditions have the average values.

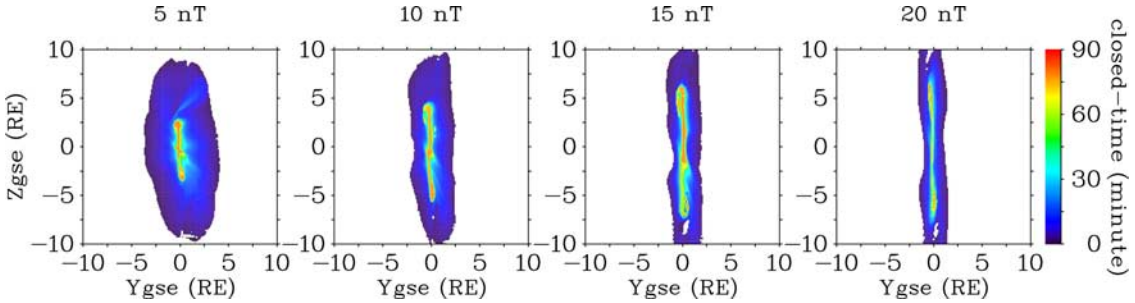

Figure 11. Solar wind entry windows located before the bowshock for different IMF magnitudes. The IMF clock angle and dipole tilt are both zero. The solar wind conditions have the average values.

squeeze of the magnetotail and thus a thinner magnetotail in the dawn-dusk direction. *Maezawa et al.* [1997] deduced that although the cross section of the distant tail is nearly circular on average, it seems to be elongated slightly in a direction determined by the IMF orientation. It is possible that such a thinner magnetotail makes the high-latitude reconnection less likely for IMF flux tubes that drap the dayside magnetopause at the location near the noon-midnight meridian. The entry window for stronger IMF is thus narrower in the dawn-dusk direction.

[63] Figure 11 also shows that the entry window as well as the group A entry area are increasingly extended in the GSE z direction, as the IMF magnitude increases. Investigating the outermost closed field line passing through the subsolar point, i.e., the first new closed field line immediately resulting from an open field line, we find that its kinked section forms at a region far more tailward if the IMF is stronger. Therefore the magnetosheath flux tube cut by the double high-latitude reconnection is longer as the IMF is stronger, and thus more fluid elements entering at the northern or southern end of the entry window are captured. Consequently, the group A entry area is extended in the GSE z direction.

5.4. Solar Wind Dynamic Pressure Dependence

[64] The pressure balance between the two sides of the magnetopause determines the diameter of the magnetosphere and the standoff distance of the subsolar point from the Earth. The pressure exerted by the solar wind on the nose of the dayside magnetopause is proportional to the dynamic pressure of the solar wind. Therefore, the size of the magnetosphere will decrease as the dynamic pressure increases. As shown in Figure 13, a smaller magnetosphere size will thus lead to a smaller size of entry window because the captured IMF flux tube is shorter. On the other hand, the entry window seems to be wider in the GSE y direction as the dynamic pressure increases. The increased width occurs because the flow path of the fluid element with higher dynamic pressure is closer to the Earth, and thus the FIMFL is more likely to reconnect with the geomagnetic field than one with the same starting position but lower dynamic pressure, as shown in Figure 14. Therefore, the overall effect of increasing dynamic pressure on the area of the entry window is small, as indicated by frames d and e in Figure 7, in which the area decreases just slightly with increasing solar wind speed or solar wind density.

[65] For low (<∼400 km/s) and high (>∼800 km/s) solar wind speed, the window size may not decrease linearly with increasing solar wind speed as shown in frame d of Figure 7. The uncertainty of the window size is high for low or high solar wind speed, suggesting that properties other than solar wind dynamic pressure, such as Mach number and plasma β, may also affect the entry window.

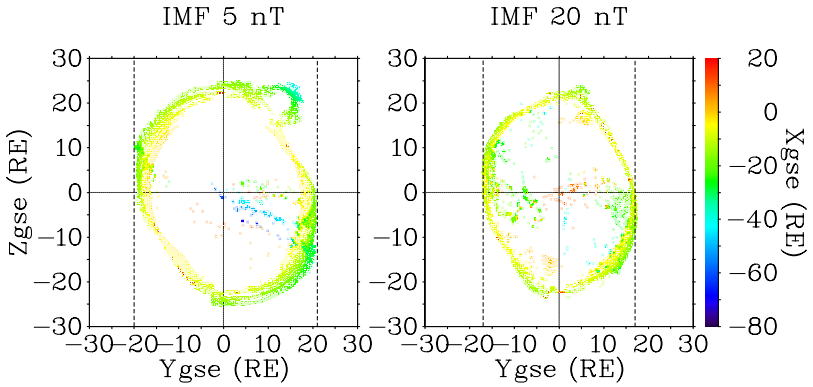

Figure 12. Two examples of the distribution of captured fluid elements at the stage when their FIMFL changes from closed to open, or when the tracing of the fluid element ends. These two plots are the same kind of plot as the one shown in frame 7 of Figure 2. The IMF direction and geomagnetic dipole direction are both pure northward. The vertical dash lines indicate the dawn or dusk edge of the magnetopause boundary in the tail.

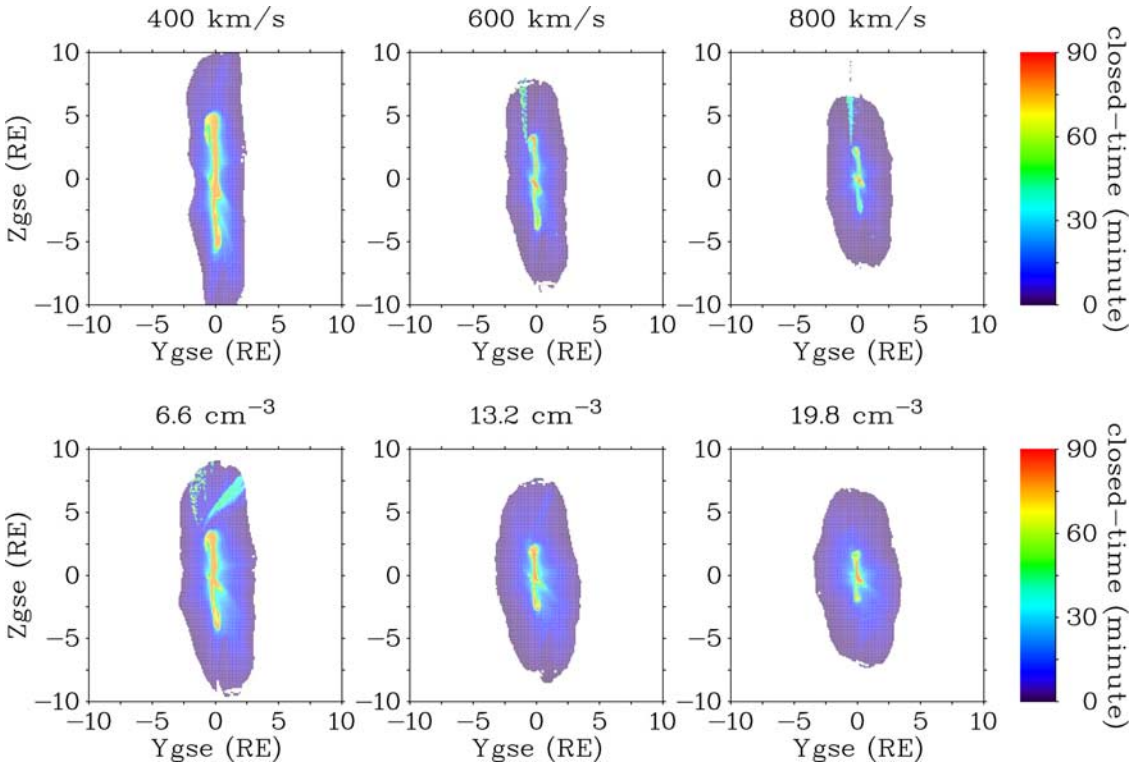

Figure 13. Solar wind entry windows located before the bowshock for different solar wind speed and density. The IMF clock angle and dipole tilt are both zero. The upper row entry windows have a solar wind density of 6.6 cm^{-3}, and the lower row entry windows have a solar wind velocity of 450 km/s.

5.5. Solar Wind Entry Rate

[66] Although there may be other mechanisms of solar wind entry into the magnetosphere under northward IMF conditions such as diffusive processes, we consider the double high-latitude reconnection mechanism as the dominant process because it is sufficient to form the cold dense plasma sheet in our simulation. We now estimate the solar wind plasma entry rate by measuring the amount of plasma that is captured by double high-latitude reconnection per unit time. Specifically for our simulation, the entering plasma per unit time is the product of the entry window area, the solar wind speed, and the solar wind density at a location before the bowshock for constant uniform solar wind and IMF conditions.

[67] This estimation avoids the use of detailed information on how the solar wind plasma entry occurs and also does not require a detailed analysis of the reconnection process itself (i.e., the reconnection rate). The distribution of velocity and density on the separatrix surface is not uniform. The plasma passing the entry window located before the bowshock at the same time may not enter across the separatrix at the same time. However, as long as the entry is relatively steady and the window size is relatively constant, this estimate will be a good approximation of the simulated actual plasma entry rate. We have computed the entry window for a number of different launching times during a simulation. We find that the entry window sizes at a certain time period only differ by small amounts except for simulations with extreme conditions. Therefore, we may assume that the plasma entry is more or less continuous for average constant solar wind and IMF conditions.

[68] Strictly speaking, we may only consider the A and B groups of the plasma fluid elements discussed in section 4.2 to be the plasma that effectively enters the magnetosphere, because the fluid elements of the C group stay only on the closed field lines on the magnetopause boundary for a short period of time. In our computation, we require 30 min of closed time as the criterion to determine if a fluid element belongs to the third group or not, based on the closed time distributions shown in Figure 3. Figure 15 summarizes the variation of the entry window area for the A−B groups and the entry rate represented by particle flux through the corresponding window area with respect to geomagnetic dipole tilt angle, solar wind, and IMF conditions. The

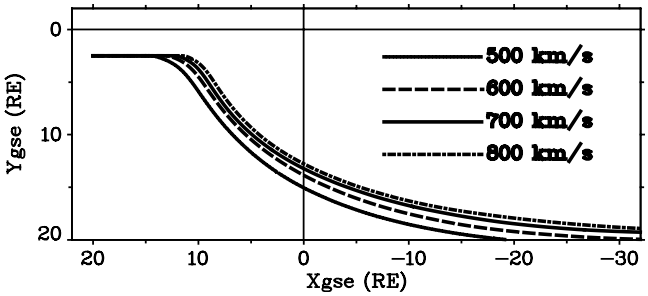

Figure 14. GSE XY plane projection of flow paths computed with the same launching position (20, 2.5, 0) R_E and the same launching time, but from simulations with different solar wind speeds. All other geospace conditions are the same, and both IMF and dipole are pure northward in these simulations.

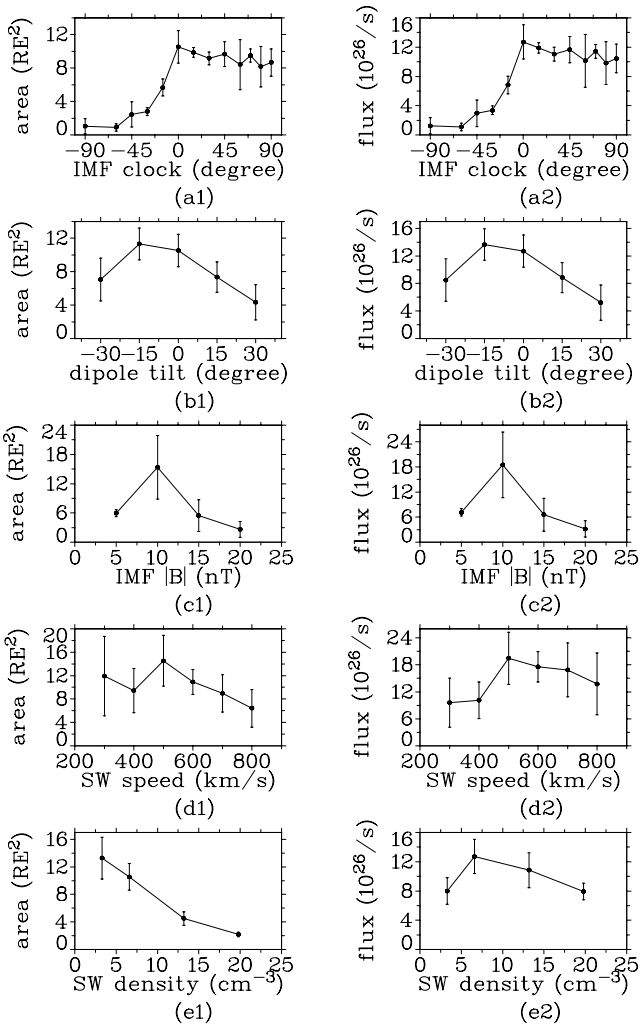

Figure 15. (left) Variation of entry window's area of the fluid elements with closed-time longer than 30 min, corresponding to frames in Figure 7. (right) Corresponding variation of entry rate, which is a product of the area shown in left frames, the solar wind density and the solar wind speed. For parameter study of IMF clock angle, dipole tilt angle, and IMF magnitude, the solar wind density is set to be 6.6 cm^{-3}, and the solar wind speed is set to be 450 km/s.

variation of the particle flux shown in Figure 15 indicates that the solar wind entry rate is of the order of 10^{26} to 10^{27} particles per second.

[69] Frames a1 and a2 of Figure 15 show that a pure north IMF clock angle maximizes plasma entry. Figure 7a shows a rather symmetric distribution of window size for entry windows with all A–C groups with respect to the IMF clock angle. However, the IMF with positive clock angle leads to a larger effective entry rate than the IMF with negative clock angle, as shown in frames a1 and a2 of Figure 15. This asymmetry is due to the ionosphere control of convection and will be discussed further below. For a large positive IMF clock angle, there is still a significant amount of solar wind plasma entering the magnetosphere.

[70] Frames b1 and b2 of Figure 15 suggest that the entry rate is maximum when the geomagnetic dipole tilts antisunward for a small angle instead of a zero angle, as a result of the reason given in section 5.2.

[71] For the typical solar wind conditions discussed in section 2, the solar wind entry is most efficient when the IMF magnitude is of the order of 10 nT, as shown in frames c1 and c2 of Figure 15. It appears that a stronger IMF leads to more A–B group fluid elements, shown in Figure 12, as a result of a longer magnetosheath flux tube that is cut by the double high-latitude reconnection (section 5.3). When the IMF is so strong that the entry window becomes very narrow, the entry rate is reduced.

[72] The entry rate maximizes as a function of solar wind speed when the solar wind speed is ~500 km/s, as indicated in frames d1 and d2 of Figure 15. It seems that high solar wind speed (>500 km/s) leads to fewer A–B group fluid elements. When the solar wind speed is greater than ~500 km/s, the decrease of the window area associated with the A–B group fluid elements is more significant than the increase of the solar wind speed. Thus the entry rate decreases slightly as the solar wind speed increases. Note that other solar wind and IMF conditions are set to average values mentioned in section 2.

[73] Frames e1 and e2 of Figure 15 show that the solar wind entry rate also has a maximum value related to the solar wind density at about 6.6 cm^{-3}. This maximum entry rate occurs because higher plasma density lets more plasma enter through the window per unit time but also leads to a smaller entry window because of higher solar wind dynamic pressure. The entry rate consequently will reach a maximum when the density increases to a certain value.

[74] In the present study the entry window and entry rate are computed after the IMF has been northward for at least two hours. Shortly after the IMF's turning from southward to northward, the plasma and field configuration near the cusp area may be significantly different from the configuration found at a later time because the magnetosphere is mostly open and more dynamic in electromagnetic and fluid properties when the IMF is southward. The size and shape of the entry window (as the one shown in Figure 16) and consequently the entry rate at the beginning of northward IMF conditions may be significantly different from those several hours later.

[75] In summary, the entry rate into the magnetosphere under northward IMF is on the order of 10^{26} to 10^{27} particles per second under constant typical solar wind and IMF conditions. However, the entry rate does not vary monotonically with most solar wind and IMF parameters but shows distinct and unexpected maxima for certain parameter values. Although we have not investigated all possible parameter combinations, the plasma entry rate maximizes at −15° geomagnetic dipole tilt, zero IMF clock angle, 10 nT IMF magnitude, 500 km/s solar wind speed, and 6.6 cm^{-3} solar wind density.

5.6. Effect of the Ionosphere

[76] In the present study, the simulations are run with the OpenGGCM version that is coupled with CTIM, the NOAA Coupled Thermosphere Ionosphere Model [*Fuller-Rowell et al.*, 1996]. The magnetosphere model provides the electron precipitation parameters and the ionosphere potential to CTIM. In turn, CTIM provides the ionospheric conductance and the ionospheric dynamo current to the magnetosphere.

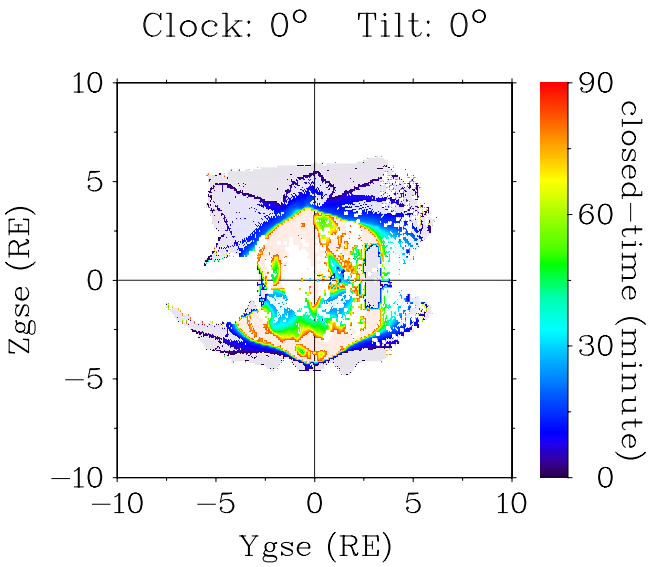

Figure 16. Solar wind entry window located before the bowshock at a time right after the IMF direction switch from southward to northward. The simulation is the same as the one used to compute the entry windows in Figure 2.

OpenGGCM can also be run without CTIM. In this case, the ionospheric conductance is set to be a constant uniform value or a built-in self-consistent model is employed.

[77] Comparing results between simulations with CTIM and simulations with constant ionospheric conductance, we find that the ionosphere has a significant effect on the entry window. For simulations with constant ionospheric conductance, the area of the entry window and the distribution of the closed time on the window are more stable and more symmetric with respect to the orientation of the IMF, as shown in Figure 17. When the ionosphere conductance is uniform and constant, the entry rate and the corresponding effective entry window (discussed in section 5.5) are symmetric with respect to positive and negative IMF clock angles. For example, the effective entry window for an IMF clock angle of 30° and −30° are 1.24 ± 0.21 R_E^2 and 1.20 ± 0.15 R_E^2, respectively. By contrast, the corresponding values shown in frame a1 of Figure 15 are 9.16 ± 0.77 R_E^2 and 2.79 ± 0.49 R_E^2, respectively. Different conductance of the ionosphere thus results in a different size of entry window. This is likely the result of different reconnection rates for different ionosphere conductance.

[78] The total entry window area is rather symmetric between the positive and negative IMF clock angle for simulations with or without CTIM. However, the symmetry of an effective entry window is broken for simulations with CTIM, as shown in frames a1 and a2 of Figure 15, but is preserved for simulations without CTIM. The effective entry window is the window through which the fluid elements stay on a newly created closed-field line longer than 30 min. For positive IMF clock angles, it seems that more captured fluid elements stay long (>30 min) on closed field lines. In other words, many new-closed field lines that have been convected to the nightside (new-closed1 field lines) for a negative IMF clock angle become open earlier (<30 min) than those for a positive IMF clock angle. Thus, in simulations with CTIM, many new-closed1 field lines for a positive IMF clock angle participate in the next high-latitude reconnection at a later time than those for a negative IMF clock angle.

[79] The convection behavior of the captured fluid element discussed in section 4.2 may explain the asymmetric behavior. The captured fluid elements flow southward (northward) and tailward on the dusk (dawn) side for both a positive and negative IMF clock angle. That means the new-closed1 field lines are convected southward (northward) and tailward on the dusk (dawn) side. Consequently, the southern (northern) section of the new-closed1 field line on the dusk (dawn) side will come close to the southern (northern) magnetotail boundary, but the northern (southern) section of the new-closed1 field line on the dusk (dawn) side is not close to the northern (southern) magnetotail boundary and is covered by a layer of open field. The closed1 field line in Figure 1 is an example in the duskside. Such distribution of new-closed1 field lines in the tail will let the merging IMF field lines with a positive clock angle have a smaller chance to connect with the new-closed1 field lines, because the merging IMF field lines will most likely connect with open field lines on the northern tail boundary on the duskside and on the southern tail boundary on the dawn side. In the opposite case, the IMF field lines with a negative clock angle are most likely aligned with the new-

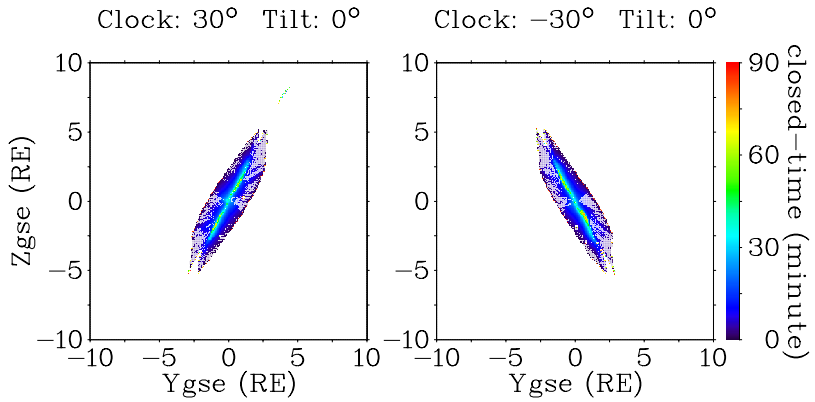

Figure 17. Solar wind entry windows located before the bowshock for IMF clock angles of 30° and −30° computed from simulations with constant uniform ionosphere conductance.

closed1 field lines, and have more chance to reconnect with them. Therefore, the new-closed1 field line created from IMF with a positive clock angle has less chance for reconnection, and has better chance to stay closed for a longer time (>30 min).

[80] In the simulations with constant uniform ionosphere conductance, the convection behavior is symmetric with respect to negative and positive IMF clock angle. That is, the new-closed1 field lines are convected southward (northward) and tailward on the dusk (dawn) side only for a negative IMF clock angle. For a positive IMF clock angle, the new-closed1 field lines are convected northward (southward) and tailward on the duskside (dawnside). Consequently, the effective entry window is symmetric with respect to negative and positive IMF clock angle and has smaller size than the one with CTIM.

[81] *Atkinson and Hutchison* [1978] showed that the day-night conductivity gradient in the polar cap E region of the ionosphere redirects the antisunward convective flow to the dawnside of the polar cap. The magnitude of the effect increases with the increasing conductivity gradient. They showed that this causes the lack of mirror symmetry in the flow pattern. The Region 1 Birkeland current pattern has been found to rotate longitudinally during periods with strong IMF B_y [*Erlandson et al.*, 1988; *Zhou et al.*, 2000]. Since the currents in the ionosphere, the field aligned currents and the currents on the magnetopause (Chapman-Ferraro currents), are all connected, and the plasma flow convection is affected by $\mathbf{J} \times \mathbf{B}$ force, the ionosphere may cause the asymmetry found in this study through the current system.

[82] The present simulations for parameter study show a higher effective entry rate for a positive IMF clock angle. However, we cannot rule out that there are certain conditions that may lead to the opposite result because the convection behavior is affected by several factors, such as IMF clock angle, solar wind conditions, ionosphere, and the magnetopause boundary layer with open field. One example of the opposite convection behavior is shown in the plot in Figure 5 for the CDPS event on 23 October 2003, comparing to frame 4 of Figure 2. It is possible that the ionosphere tends to cause a higher effective entry rate for a positive IMF clock angle, but some other factors, such as solar wind conditions, may cause the opposite result. When such factors are sufficiently strong, the convection behavior will become opposite to that caused by the ionospheric effects. Further parametric studies will resolve this issue, but are beyond the scope of this paper.

[83] CTIM provides a much more realistic ionosphere compared to a uniform-conductance ionosphere model [*Raeder et al.*, 2001b]. Therefore, our simulation shows that in the real world the ionosphere has a significant effect on the convection of the entering solar wind plasma and consequently affects the high-latitude reconnection rate and the solar wind entry rate with respect to different IMF clock angles.

6. Summary and Discussion

[84] Following a successful event study [*Li et al.*, 2005], we have simulated the magnetosphere with the global MHD model OpenGGCM for various solar wind conditions, northward IMF clock angles, and geomagnetic dipole tilt angles. In our analysis, we trace the solar wind plasma flow globally, and study the fluid elements' flow paths and the magnetic field lines threading through the fluid elements. We construct solar wind entry windows to display how the solar wind plasma enters the magnetosphere and estimate the entry rate with respect to various conditions.

[85] Our simulations show that high-latitude reconnection occurs between IMF field lines and lobe field lines, between IMF field lines and new-closed field lines that have been convected to the nightside, between new-open field lines and lobe field lines, and between new-open field lines and nightside new-closed field lines. Such high-latitude reconnection processes are listed in Table 2. High-latitude reconnection occurs for any IMF clock angle between $-90°$ and $90°$, and for any geomagnetic dipole tilt between $-30°$ and $30°$. Under constant northward IMF conditions, high-latitude reconnection continuously converts lobe/mantle open field lines into closed field lines and also converts newly created closed field lines that have been convected to the nightside back into open field lines. An IMF field line with zero x component usually first reconnects with a geomagnetic field line at the northern high-latitude boundary when the geomagnetic dipole tilts positive toward the Sun, and in the opposite hemisphere for negative dipole tilt.

[86] IMF flux tubes near the dayside magnetopause are deformed by $\mathbf{J} \times \mathbf{B}$ force. This deformation makes the effective clock angle smaller for an IMF field line near the magnetopause with originally large clock angle ($70°-90°$), thus facilitating the reconnection of IMF field lines that are oriented close to the dawn-dusk direction.

[87] Double high-latitude reconnection captures magnetosheath plasma and brings it into the magnetosphere. Under constant northward IMF conditions, there is an entry window through which solar wind plasma flows into the magnetosphere, resulting from double high-latitude reconnection. The entering solar wind plasma can be classified by dividing it into three parts. The first part (group A) enters the dayside inner magnetosphere and the plasma sheet. The second part (group B) flows to near the tail magnetopause. The third part (group C) also flows to the near-tail magnetopause, but stays on the closed field just for a relatively short period (<30 min). The convection behavior of the entering solar wind plasma depends on the IMF clock angle, dipole tilt angle, solar wind conditions, ionosphere conductance, and distribution of the open field close to the magnetopause.

[88] The path and destination of the entering magnetosheath plasma determines the distribution of cold dense plasma in the magnetosphere. The entering plasma of group A is the main source of the cold dense plasma sheet, which is most likely to form in the near-magnetotail flanks. Some of the group A entering plasma stays in the dayside inner magnetosphere. The path and destination of the B and C groups of entering plasma indicate that there is also cold dense plasma distributed adjacent to the near-magnetotail magnetopause. Such cold dense plasma is located on closed field lines and is denser and flows faster than the cold dense plasma in the plasma sheet.

[89] Double high-latitude reconnection not only captures magnetosheath plasma but also simultaneously releases some of the captured plasma that has convected to the

nightside. Cold dense plasma may also diffuse into neighboring regions. Therefore, a balance between inflow and outflow of cold dense plasma is established at some point under constant northward IMF conditions. Such capture-release process also implies a geomagnetic field convection cycle from open to close and back to open.

[90] Our simulation reveals the variation of the entry window before the bowshock with respect to the geomagnetic dipole tilt, solar wind, and IMF conditions. The area of the entry window decreases as the magnitude of the IMF clock angle increases. The orientation of the entry window aligns with the IMF clock angle. The entry window for a larger dipole tilt tends to be smaller. A stronger IMF leads to a thinner entry window in the GSE y direction. As solar wind dynamic pressure increases, the entry window becomes smaller and wider in the GSE y direction.

[91] We estimate the solar wind plasma entry rate to be of the order of 10^{26} to 10^{27} particles per second on the basis of the influx of the A−B group plasma elements. The entry rate is represented by the flux of the A and B group entering plasma. The entry rate peaks when the IMF clock angle is $\sim 0°$, the dipole tilt angle is $\sim -15°$, the IMF magnitude is $\sim$10 nT, the solar wind speed is $\sim$500 km/s, and the solar wind density is $\sim$6.6 cm^{-3}.

[92] Our simulations with different ionosphere conductance models indicate that the ionosphere conductance affects the convection behavior of the newly closed field lines and consequently causes asymmetry in the effective entry rate with respect to the IMF clock angle.

[93] Our simulation results are comparable with several observations. First of all, the occurrence of high-latitude reconnection has early been proposed [*Dungey*, 1963; *Russell*, 1972; *Cowley*, 1981]. Observations have provided evidence [e.g., *Gosling et al.*, 1991; *Kessel et al.*, 1996; *Fuselier et al.*, 2000; *Le et al.*, 2001; *Onsager et al.*, 2001; *Lavraud et al.*, 2002; *Phan et al.*, 2003; *Lavraud et al.*, 2005a], and global MHD numerical simulation models have reproduced this process [*Ogino et al.*, 1994; *Fedder and Lyon*, 1995; *Raeder et al.*, 1997; *Gombosi et al.*, 1998; *Guzdar et al.*, 2001]. *Onsager et al.* [2001] reported a broad local time range of reconnection locations near the cusp. Our entry windows for IMF clock angles between −90° and 90° suggest that the reconnection location is not limited around midnight tailward of cusp. The reconnection location may be near the flanks as well. Reconnection near the northern dawnside flank under northward IMF condition has also been reported by *Eriksson et al.* [2004]. *Onsager et al.* [2001] has identified all the characteristic field lines that result from high-latitude reconnection: new open field lines with footprints in either northern or southern hemisphere, new closed field lines, and high-latitude closed field lines participating in high-latitude reconnection. Using our nomenclature, these are the open2, closed2, and high-latitude closed1 field lines, respectively, that have been analyzed in the present study.

[94] *Twitty et al.* [2004] found that cusp reconnection can occur for IMF clock angles, as measured by ACE, between −90° and 90°. Our entry windows shown in Figure 8 support this finding. On the other hand, *Lavraud et al.* [2006] discovered that the high-latitude reconnection occurs primarily when the magnetosheath magnetic field line clock angle, measured by Cluster FGM, lies in the interval [−60°,60°]. This observation can be explained by our simulation result that reveals the deformation of the magnetosheath flux tube approaching the dayside magnetopause by $\mathbf{J} \times \mathbf{B}$ force. We observe in our simulation that pure B_y IMF flux tubes are tilted to a clock angle near 60° at the magnetopause and reconnect with geomagnetic flux tubes. The results of *Lavraud et al.* [2006], as they note, were also potentially affected by orbital effects, owing to Cluster sampling primarily high-latitude regions. *Crooker et al.* [1998] also showed in a MHD simulation that the pure B_y IMF field lines drape over the noon meridian, rather than the equator, and merge with geomagnetic field lines.

[95] *Lavraud et al.* [2005b] showed that an IMF flux tube will first participate in high-latitude reconnection at the northern (southern) hemisphere, and then at southern (northern) hemisphere, when the geomagnetic dipole tilts sunward (antisunward), even for IMF with a nonzero x component. We find the same phenomenon for IMF with a zero x component in our simulations for dipole tilt angles of +15°, +30°, −15°, and −30° in the GSE XZ plane.

[96] At the dayside magnetopause, a layer of newly open field lines and a layer of newly closed field lines are indicated by entry windows at the magnetopause, shown in Figure 2. Such layers have been identified by *Le et al.* [1996] and *Onsager et al.* [2001].

[97] The entering solar wind fluid elements of group B flow to the near-tail magnetopause. The plasma of this group thus forms a boundary layer in the magnetotail. *Raeder et al.* [1997] proposed a so called tail flank boundary layer (TFBL) under northward IMF conditions based on global simulations and Geotail observations. Geotail observed plasma near $X_{gse} = -46$ R_E with a slow tailward speed and on closed field lines.

[98] Our simulation reproduces a cold dense plasma sheet that has the observed level of density and temperature. Its location and distribution are also consistent with observations, which show that the CDPS is mainly near the tail flanks but can also be found deep inside the plasma sheet [e.g., *Fujimoto et al.*, 1996, 1998; *Phan et al.*, 1998; *Fuselier et al.*, 1999; *Øieroset et al.*, 2002].

[99] During the long period northward IMF event on 23 October 2003, Cluster observed the transition from a hot tenuous plasma sheet to a cold dense plasma sheet, with density staying at the 1.5 cm^{-3} level [*Øieroset et al.*, 2005]. This transition took about 3 h of northward IMF. To estimate the time needed to form the cold dense plasma sheet in the simulation, we assume one piece of the CDPS near one side of the tail flank to be 30 R_E long in X_{gse}, 10 R_E wide in Y_{gse}, and 5 R_E high in Z_{gse}. This volume estimate is based on the statistical spatial distribution of CDPS presented by *Fujimoto et al.* [2002]. The total volume of the two pieces of CDPS is $\sim 8 \times 10^{29}$ cm^3. Assuming the CDPS density is $\sim$1.5 cm^{-3} and the net entry flux is $\sim 1 \times 10^{26}$ particles per second, it will take $\sim$3 h to fill the volume. Although this is a rather rough estimate, it must be noted that our simulation for this period has almost the same transition time from a hot tenuous plasma sheet to a cold dense plasma sheet.

[100] The Kelvin-Helmholtz instability (KHI) has been proposed as a process that enhances diffusivity, and facilitates local mass transport and ion mixing, at the flanks of the magnetopause under northward IMF conditions [*Fujimoto*

and Terasawa, 1994; *Nykyri and Otto*, 2001; *Nykyri et al.*, 2006; *Hasegawa et al.*, 2004]. In our simulation, we do not see any KHI signatures, possibly as the result of insufficient grid resolution, which decreases in GSE x direction as the computation advances to the tail. However, KHI and high-latitude reconnection are not mutually exclusive as a solar wind entry mechanism. It is possible that KHI contributes a significant amount of magnetosheath plasma to the magnetosphere. The relation between the entry rate and the solar wind speed or density in the present study may help spacecraft in situ observations discriminate between the two processes, for instance, if KHI is assumed to increase plasma entry with increasing solar wind velocity and/or density.

[101] **Acknowledgments.** The authors would like to thank Tai Phan, Marit Øieroset, and Don Fairfield for many useful discussions. The work at UNH was supported by LANL IGPP mini-grant 1518, by grant ATM-0503189 from the National Science Foundation GEM program, and by NASA grant SECGI P04-0025-O171. Computations were performed on the Zaphod Beowulf cluster which was in part funded by the Major Research Instrumentation program of the National Science Foundation under grant ATM-0420905.

[102] Wolfgang Baumjohann thanks Stefan Eriksson and another reviewer for their assistance in evaluating this paper.

References

Atkinson, G., and D. Hutchison (1978), Effect of the day night ionospheric conductivity gradient on polar cap convective flow, *J. Geophys. Res.*, *83*, 725.

Axford, W. I., and C. O. Hines (1961), A unifying theory of high latitude geophysical phenomena and geomagnetic storms, *Can. J. Phys.*, *39*, 1433.

Baumjohann, W., G. Paschmann, and C. A. Cattell (1989), Average plasma properties in the central plasma sheet, *J. Geophys. Res.*, *94*, 6597.

Bobra, M. G., S. M. Petrinec, S. A. Fuselier, E. S. Claflin, and H. E. Spence (2004), On the solar wind control of cusp aurora during northward IMF, *Geophys. Res. Lett.*, *31*, L04805, doi:10.1029/2003GL018417.

Chandler, M. O., S. A. Fuselier, M. Lockwood, and T. E. Moore (1999), Evidence of component merging equatorward of the cusp, *J. Geophys. Res.*, *104*, 22,623.

Cowley, S. W. H. (1980), Plasma populations in a simple open model magnetosphere, *Space Sci. Rev.*, *26*, 217.

Cowley, S. W. H. (1981), Magnetospheric and ionospheric flow and the interplanetary magnetic field, in *The Physical Basis of the Ionosphere in the Solar-Terrestrial System*, *AGARD Conf. Proc.*, *295*, 4/1–4/14.

Cowley, S. W. H. (1983), Interpretation of observed relations between solar wind characteristics and effects at ionospheric altitudes, in *High Latitude Space Plasma Physics*, edited by B. Hultquist and T. Hagfors, p. 225, Plenum, New York.

Crooker, N. U. (1992), Reverse convection, *J. Geophys. Res.*, *97*, 19,363.

Crooker, N. U., J. G. Lyon, and J. A. Fedder (1998), MHD model merging with IMF B_y: Lobe cells, sunward polar cap convection, and overdraped lobes, *J. Geophys. Res.*, *103*, 9143.

Dungey, J. W. (1961), Interplanetary magnetic field and the auroral zones, *Phys. Rev. Lett.*, *6*, 47.

Dungey, J. W. (1963), The structure of the exosphere or adventures in velocity space, in *Geophysics, The Earth's Environment*, edited by C. DeWitt, J. Hieblot, and A. Lebeau, p. 550, Gordon and Breach, Newark, N. J.

Eastman, T. E., B. Popielawska, and L. A. Frank (1985), Three-dimensional plasma observations near the outer magnetospheric boundary, *J. Geophys. Res.*, *90*, 9519.

Eriksson, S., S. R. Elkington, T. D. Phan, S. M. Petrinec, H. Rème, M. W. Dunlop, M. Wiltberger, A. Balogh, R. E. Ergun, and M. André (2004), Global control of merging by the interplanetary magnetic field: Cluster observations of dawnside flank magnetopause reconnection, *J. Geophys. Res.*, *109*, A12203, doi:10.1029/2003JA010346.

Erlandson, R. E., L. J. Zanetti, T. A. Potemra, P. F. Bythrow, and R. Lundin (1988), IMF By dependence of region 1 Birkeland currents near noon, *J. Geophys. Res.*, *93*, 9804.

Fairfield, D. H., R. P. Lepping, E. W. Hones, S. J. Bame, and J. R. Asbridge (1981), Simultaneous measurements of magnetotail dynamics by IMP spacecraft, *J. Geophys. Res.*, *86*, 1396.

Fairfield, D. H., A. Otto, T. Mukai, S. Kokubun, R. P. Lepping, J. T. Steinberg, A. J. Lazarus, and T. Yamamoto (2000), Geotail observations of the Kelvin-Helmholtz instability at the equatorial magnetotail boundary for parallel northward fields, *J. Geophys. Res.*, *105*, 21,159.

Fedder, J. A., and J. G. Lyon (1995), The Earth's magnetosphere is 165 R_E long: Self-consistent currents, convection, magnetospheric structure, and processes for northward interplanetary magnetic field, *J. Geophys. Res.*, *100*, 3623.

Fujimoto, M., and T. Terasawa (1994), Anomalous ion mixing within an MHD scale Kelvin-Helmholtz vortex, *J. Geophys. Res.*, *99*, 8601.

Fujimoto, M., A. Nishida, T. Mukai, Y. Saito, T. Yamamoto, and S. Kokubun (1996), Plasma entry from the flanks of the near-Earth magnetotail: Geotail observations in the dawnside LLBL and the plasma sheet, *J. Geomagn. Geoelectr.*, *48*, 711.

Fujimoto, M., T. Terasawa, T. Mukai, Y. Saito, T. Yamamoto, and S. Kokubun (1998), Plasma entry from the flanks of the near-Earth magnetotail: Geotail observations, *J. Geophys. Res.*, *103*, 4391.

Fujimoto, M., T. Mukai, and S. Kokubun (2002), The structure of the plasma sheet under northward IMF, in *Frontiers in Magnetospheric Plasma Physics*, edited by M. Hoshino, Y. Omura, and L. J. Lanzerotti, COSPAR, Kanagawa, Japan.

Fuller-Rowell, T. J., D. Rees, S. Quegan, R. J. Moffett, M. V. Codrescu, and G. H. Millward (1996), A coupled thermosphere-ionosphere model (CTIM), in *STEP Report*, edited by R. W. Schunk, p. 217, NOAA, Boulder, Colo.

Fuselier, S. A., B. J. Anderson, and T. G. Onsager (1997), Electron and ion signatures of field line topology at the low-shear magnetopause, *J. Geophys. Res.*, *102*, 4847.

Fuselier, S. A., R. C. Elphic, and J. T. Gosling (1999), Composition measurements in the dusk flank magnetosphere, *J. Geophys. Res.*, *104*, 4515.

Fuselier, S. A., K. J. Trattner, and S. M. Petrinec (2000), Cusp observations of high- and low-latitude reconnection for northward interplanetary field, *J. Geophys. Res.*, *105*, 253.

Gombosi, T. I., D. L. DeZeeuw, C. P. T. Groth, K. G. Powell, and P. Song (1998), The length of the magnetotail for northward IMF: Results of 3D MHD simulations, *Phys. Space Plasmas*, *15*, 121.

Gosling, J. T., M. F. Thomsen, S. J. Bame, and R. C. Elphic (1991), Observations of reconnection of interplanetary and lobe magnetic field lines at the high-latitude magnetopause, *J. Geophys. Res.*, *96*, 14,097.

Guzdar, P. N., X. Shao, C. C. Goodrich, K. Papadopoulos, M. J. Wiltberger, and J. G. Lyon (2001), Three-dimensional MHD simulations of the steady state magnetosphere with northward interplanetary magnetic field, *J. Geophys. Res.*, *106*, 275.

Hasegawa, H., M. Fujimoto, T. D. Phan, H. Rème, A. Balogh, M. W. Dunlop, C. Hashimoto, and R. TanDokoro (2004), Transport of solar wind into Earth's magnetosphere through rolled-up Kelvin-Helmholtz vortices, *Nature*, *430*, 755.

Hultqvist, B., M. Andre, S. P. Christon, G. Paschmann, and D. G. Sibeck (1999), Contributions of different source and loss processes to the plasma content of the magnetosphere, *Space Sci. Rev.*, *88*, 355.

Imber, S. M., S. E. Milan, and B. Hubert (2006), The auroral and ionospheric flow signatures of dual lobe reconnection, *Ann. Geophys.*, *24*, 3115.

Kessel, R. L., S.-H. Chen, J. L. Green, S. F. Fung, S. A. Boardsen, L. C. Tan, T. E. Eastman, J. D. Craven, and L. A. Frank (1996), Evidence of high-latitude reconnection during northward IMF: Hawkeye observations, *Geophys. Res. Lett.*, *23*, 583.

Kivelson, M. G., and C. T. Russell (1995), *Introduction to Space Physics*, Cambridge Univ. Press, Cambridge, U.K.

Knipp, D. J. (1993), Ionospheric convection response to slow, strong variations in a northward interplanetary magnetic field: A case study for January 14, 1988, *J. Geophys. Res.*, *98*, 19,273.

Lavraud, B. (2002), et al., Cluster observations of the exterior cusp and its surrounding boundaries under northward IMF, *Geophys. Res. Lett.*, *29*(20), 1995, doi:10.1029/2002GL015464.

Lavraud, B., et al. (2004), The exterior cusp and its boundary with the magnetosheath: Cluster multi-event analysis, *Ann. Geophys.*, *22*, 3039.

Lavraud, B., A. Fedorov, E. Budnik, M. F. Thomsen, A. Grigoriev, P. J. Cargill, M. W. Dunlop, H. Rème, I. Dandouras, and A. Balogh (2005a), High-altitude cusp flow dependence on IMF orientation: A 3-year Cluster statistical study, *J. Geophys. Res.*, *110*, A02209, doi:10.1029/2004JA010804.

Lavraud, B., M. F. Thomsen, M. G. G. T. Taylor, Y. L. Wang, T. D. Phan, S. J. Schwartz, R. C. Elphic, A. Fazakerley, H. Rème, and A. Balogh (2005b), Characteristics of the magnetosheath electron boundary layer under northward interplanetary magnetic field: Implications for high-latitude reconnection, *J. Geophys. Res.*, *110*, A06209, doi:10.1029/2004JA010808.

Lavraud, B., M. F. Thomsen, B. Lefebvre, S. J. Schwartz, K. Seki, T. D. Phan, Y. L. Wang, A. Fazakerley, H. Rème, and A. Balogh (2006), Evidence for newly closed magnetosheath field lines at the dayside magnetopause under northward IMF, *J. Geophys. Res.*, *111*, A05211, doi:10.1029/2005JA011266.

Le, G., C. T. Russell, J. T. Gosling, and M. F. Thomsen (1996), ISEE observations of low-latitude boundary layer for northward interplanetary magnetic field: Implications for cusp reconnection, *J. Geophys. Res.*, *101*, 27,239.

Le, G., J. Raeder, C. T. Russell, G. Lu, S. M. Petrinec, and F. S. Mozer (2001), Polar cusp and vicinity under strongly northward IMF on April 11, 1997: Observations and MHD simulations, *J. Geophys. Res.*, *106*, 21,083.

LeMaire, J. (1977), Impulsive penetration of filamentary plasma elements into the magnetospheres of the Earth and Jupiter, *Planet. Space Sci.*, *25*, 887.

Lennartsson, W. (1992), A scenario for solar wind penetration of Earth's magnetic tail based on ion composition data from the ISEE 1 spacecraft, *J. Geophys. Res.*, *97*, 19,221.

Li, W., J. Raeder, J. Dorelli, M. Øieroset, and T. D. Phan (2005), Plasma sheet formation during long period of northward IMF, *Geophys. Res. Lett.*, *32*, L12S08, doi:10.1029/2004GL021524.

Lin, Y., and X. Y. Wang (2006), Formation of dayside low-latitude boundary layer under northward interplanetary magnetic field, *Geophys. Res. Lett.*, *33*, L21104, doi:10.1029/2006GL027736.

Maezawa, K. (1976), Magnetospheric convection induced by the positive and negative Z components of the interplanetary magnetic field: Quantitative analysis using polar cap magnetic records, *J. Geophys. Res.*, *81*, 2289.

Maezawa, K., T. Hori, T. Mukai, Y. Saito, T. Yamamoto, S. Kokubun, and A. Nishida (1997), Structure of the distant magnetotail and its dependence on the IMF By component: GEOTAIL observations, *Adv. Space Res.*, *20*, 949.

Matsuoka, A., K. Tsuruda, H. Hayakawa, T. Mukai, and A. Nishida (1996), Electric field structure and ion precipitation in the polar region associated with northward interplanetary magnetic field, *J. Geophys. Res.*, *101*, 10,711.

Milan, S. E., S. W. H. Cowley, M. Lester, D. M. Wright, J. A. Slavin, M. Fillingim, C. W. Carlson, and H. J. Singer (2004), Response of the magnetotail to changes in the open flux content of the magnetosphere, *J. Geophys. Res.*, *109*, A04220, doi:10.1029/2003JA010350.

Nishikawa, K. I. (1998), Particle entry through reconnection grooves in the magnetopause with a dawnward IMF as simulated by a 3-D EM particle code, *Geophys. Res. Lett.*, *25*, 1609.

Nykyri, K., and A. Otto (2001), Plasma transport at the magnetospheric boundary due to reconnection in Kelvin-Helmholtz vortices, *Geophys. Res. Lett.*, *28*, 3565.

Nykyri, K., A. Otto, B. Lavraud, C. Mouikis, L. M. Kistler, A. Balogh, and H. Rème (2006), Cluster observations of reconnection due to the Kelvin-Helmholtz instability at the dawnside magnetospheric flank, *Ann. Geophys.*, *24*, 2619.

Ogino, T., R. J. Walker, and M. Ashour-Abdalla (1994), A global magnetohydrodynamic simulation of the response of of the magnetosphere to a northward turning of the interplanetary magnetic field, *J. Geophys. Res.*, *99*, 11,027.

Øieroset, M., T. D. Phan, M. Fujimoto, L. Chan, R. P. Lin, and R. Skoug (2002), Spatial and temporal variations of the cold dense plasma sheet: Evidence for a low-latitude boundary layer source?, in *Earth's Low-Latitude Boundary Layer*, *Geophys. Monogr. Ser.*, vol. 133, edited by P. T. Newell and T. G. Onsager, p. 253, AGU, Washington, D. C.

Øieroset, M., J. Raeder, T. D. Phan, S. Wing, J. P. McFadden, W. Li, M. Fujimoto, H. Rème, and a Balogh (2005), Global cooling and densification of the plasma sheet during an extended period of purely northward IMF on October 22–24, 2003, *Geophys. Res. Lett.*, *32*, L12S07, doi:10.1029/2004GL021523.

Omelchenko, A. N., O. L. Vaisberg, and C. T. Russell (1983), Further analysis of plasma bursts in Earth's boundary layer at high latitudes, *Cosmic Res.*, *21*, 687.

Onsager, T. G., J. D. Scudder, M. Lockwood, and C. T. Russell (2001), Reconnection at the high-latitude magnetopause during northward interplanetary magnetic field conditions, *J. Geophys. Res.*, *106*, 25,467.

Peroomian, V. (2003a), Interplanetary magnetic field-dependent impact of solar wind ions on Earth's magnetopause, in *Earth's Low-Latitude Boundary Layer*, *Geophys. Monogr. Ser.*, vol. 133, edited by P. T. Newell and T. Onsager, p. 45, AGU, Washington, D. C.

Peroomian, V. (2003b), The influence of the interplanetary magnetic field on the entry of solar wind ions into the magnetosphere, *Geophys. Res. Lett.*, *30*(7), 1407, doi:10.1029/2002GL016627.

Petrinec, S. M., and C. T. Russell (1996), Near-Earth magnetotail shape and size as determined from the magnetopause flaring angle, *J. Geophys. Res.*, *101*, 137.

Phan, T. D., G. Paschmann, A. Raj, V. Angelopoulos, D. Larson, and R. P. Lin (1998), Wind observations of the halo/cold plasma sheet, in *Substorms-4*, edited by S. Kokubun and Y. Kamide, p. 219, Terra Sci., Boston, Mass.

Phan, T. D., R. P. Lin, S. A. Fuselier, and M. Fujimoto (2000), Wind observations of mixed magnetosheath-plasma sheet ions deep inside the magnetosphere, *J. Geophys. Res.*, *105*, 5497.

Phan, T. D., et al. (2003), Simultaneous Cluster and IMAGE observations of cusp reconnection and auroral proton spot for northward IMF, *Geophys. Res. Lett.*, *30*(10), 1509, doi:10.1029/2003GL016885.

Pilipp, W. G., and G. Morfill (1978), The formation of the plasma sheet resulting from plasma mantle dynamics, *J. Geophys. Res.*, *83*, 5670.

Raeder, J. (1999), Modeling the magnetosphere for northward interplanetary magnetic field: Effects of electrical resistivity, *J. Geophys. Res.*, *104*, 17,357.

Raeder, J. (2003), Global magnetohydrodynamics: A tutorial, in *Space Plasma Simulation*, edited by J. Buechner, C. T. Dum, and M. Scholer, *Lect. Not. in Phys.*, vol. 615, Springer, New York.

Raeder, J., R. J. Walker, and M. Ashour-Abdalla (1995), The structure of the distant geomagnetic tail during long periods of northward IMF, *Geophys. Res. Lett.*, *22*, 349.

Raeder, J., J. Berchem, M. Ashour-Abdalla, L. A. Frank, W. R. Paterson, K. L. Ackerson, R. P. Lepping, S. Kokubun, T. Yamamoto, and S. A. Slavin (1997), Boundary layer formation in the magnetotail: Geotail observations and comparisons with a global MHD model, *Geophys. Res. Lett.*, *24*, 951.

Raeder, J., J. Berchem, and M. Ashour-Abdalla (1998), The Geospace Environment Modeling grand challenge: Results from a Global Geospace Circulation Model, *J. Geophys. Res.*, *103*, 14,787.

Raeder, J., R. L. McPherron, L. A. Frank, W. R. Paterson, J. B. Sigwarth, G. Lu, H. J. Singer, S. Kokubun, T. Mukai, and J. A. Slavin (2001a), Global simulation of the geospace environment modeling substorm challenge event, *J. Geophys. Res.*, *106*, 381.

Raeder, J., Y. L. Wang, and T. Fuller-Rowell (2001b), Geomagnetic storm simulation with a coupled magnetosphere-ionosphere-thermosphere model, in *Space Weather*, *Geophys. Monogr. Ser.*, vol. 125, edited by P. Song, G. Siscoe, and H. J. Singer, p. 377, AGU, Washington, D. C.

Reiff, P. H., and J. L. Burch (1985), B_y-dependent dayside plasma flow and Birkeland currents in the dayside magnetosphere, II - A global model for northward and for southward IMF, *J. Geophys. Res.*, *90*, 1595.

Richard, R. L., R. J. Walker, and M. Ashour-Abdalla (1994), The population of the magnetosphere by solar winds ions when the interplanetary magnetic field is northward, *Geophys. Res. Lett.*, *21*, 2455.

Robinson, R. M., R. R. Vondrak, K. Miller, T. Dabbs, and D. Hardy (1987), On calculating ionospheric conductances from the flux and energy of precipitating electrons, *J. Geophys. Res.*, *92*, 2565.

Rosenbauer, H., H. Grunwaldt, M. D. Montgomery, G. Paschmann, and N. Sckopke (1975), Heos 2 plasma observations in the distant polar magnetosphere: The plasma mantle, *J. Geophys. Res.*, *80*, 2723.

Russell, C. T. (1972), The configuration of the magnetosphere, in *Critical Problems of Magnetospheric Physics*, edited by E. R. Dyer, p. 1, Natl. Acad. of Sci., Washington, D. C.

Sckopke, N., G. Paschmann, G. Haerendel, B. U. O. Sonnerup, S. J. Bame, T. G. Forbes, E. W. Hones, and C. T. Russell (1981), Structure of the low-latitude boundary layer, *J. Geophys. Res.*, *86*, 2099.

Sibeck, D. G., et al. (1999), Plasma transfer processes at the magnetopause, *Space Sci. Rev.*, *88*, 207.

Song, P., and C. T. Russell (1992), Model of the formation of the low-latitude boundary layer for strongly northward interplanetary magnetic field, *J. Geophys. Res.*, *97*, 1411.

Song, P., D. L. DeZeeuw, T. I. Gombosi, C. P. T. Groth, and K. G. Powell (1999), A numerical study of solar wind-magnetosphere interaction for northward interplanetary magnetic field, *J. Geophys. Res.*, *104*, 28,361.

Sonnerup, B. U. O. (1974), The magnetopause reconnection rate, *J. Geophys. Res.*, *79*, 1546.

Terasawa, T., M. Fujimoto, T. Mukai, I. Shinohara, Y. Saito, T. Yamamoto, S. Machida, S. Kokubun, A. J. Lazarus, and J. T. Steinberg (1997), Solar wind control of density and temperature in the near-earh plasma sheet: WIND/GEOTAIL collaboration, *Geophys. Res. Lett.*, *24*, 935.

Thorne, R. M., and B. T. Tsurutani (1991), *Physics of Space Plasmas*, *SPI Conf. Proc. and Reprint Ser.*, vol. 10, Scientific, Cambridge, Mass.

Trattner, K. J., S. A. Fuselier, and S. M. Petrinec (2004), Location of the reconnection line for northward interplanetary magnetic field, *J. Geophys. Res.*, *109*, A03219, doi:10.1029/2003JA009975.

Treumann, R. A., Theory of super-diffusion for the magnetopause (1997), *Geophys. Res. Lett.*, *24*, 1727.

Tsurutani, B. T., G. S. Lakhina, L. Zhang, J. S. Pickett, and Y. Kasahara (2003), ELF/VLF plasma waves in the low latitude boundary layer, in *Earth's Low-Latitude Boundary Layer*, *Geophys. Monogr. Ser.*, vol. 133, edited by P. T. Newell and T. G. Onsager, p. 189, AGU, Washington, D. C.

Twitty, C., T. D. Phan, G. Paschmann, B. Lavraud, H. Rème, and M. Dunlop (2004), Cluster survey of cusp reconnection and its IMF dependence, *Geophys. Res. Lett.*, *31*, L19808, doi:10.1029/2004GL020646.

Walker, R. J., et al. (1999), Source and loss processes in the magnetotail, *Space Sci. Rev.*, *88*, 285.

Walker, R. J., M. Ashour-Abdalla, T. Ogino, V. Peroomian, and R. L. Richard (2003), Modeling magnetospheric sources, in *Earth's Low-Latitude Boundary Layer*, *Geophys. Monogr. Ser.*, vol. 133, edited by P. T. Newell and T. Onsager, p. 33, AGU, Washington, D. C.

Zhou, X. W., C. T. Russell, and G. Le (2000), Local time and interplanetary magnetic field By dependence of field-aligned currents at high altitudes, *J. Geophys. Res.*, *105*, 2533.

B. Lavraud and M. F. Thomsen, Space Science and Applications, Los Alamos National Laboratory, Los Alamos, NM 87545, USA. (lavraud@lanl.gov; mthomsen@lanl.gov)

W. Li and J. Raeder, Space Science Center, University of New Hampshire, Morse Hall, Durham, NH 03824, USA. (wenhuil@cisunix.unh.edu; j.raeder@unh.edu)